2 Voltage and Current Measurements and Their Applications

Measuring voltage and current is the foundation of monitoring power systems. A *voltmeter* is the basic instrument to measure voltage; see Figure 2.1(a). It is wired in parallel with the two points of the circuit at which the voltage difference is intended to be measured. An ideal voltmeter would have an infinite impedance such that it would take no current. An *ammeter* is the basic instrument to measure current; see Figure 2.1(b). It is wired in series with the circuit that carries the current that is intended to be measured. An ideal ammeter would have zero impedance such that it would create no voltage drop. Detailed discussions on digital voltmeters and ammeters and their circuits are available in [74].

2.1 Instrument Transformers

It is vital to use voltmeters and ammeters that can support the range of voltage and current that they tend to measure. For example, connecting a 30 V voltmeter to a 230 V supply may blow apart the voltmeter's internal circuitry.

One option is to use voltmeters and ammeters that can support higher ranges of voltage and current. However, this option often comes at a higher cost. A common alternative option is to use instrument transformers to first *step down* voltage or current and then measure it using a voltmeter or an ammeter, respectively.

Two basic types of instrument transformers, namely the *current transformer* (CT) and the *potential transformer* (PT), are shown in Figure 2.2. They are used to measure the primary current i_1 and the primary voltage v_1, respectively, by providing the secondary current i_2 and the secondary voltage v_2 that are *proportional* to those of the electric circuit but at significantly reduced magnitudes.

2.1.1 Turn Ratio

For an ideal CT, we have

$$\frac{i_2}{i_1} = \frac{N_1}{N_2}, \tag{2.1}$$

where N_1 and N_2 indicate the number of turns in the primary and the secondary windings, respectively. Some typical turn ratios are 50:5, 100:5, 400:5, and 4000:5,

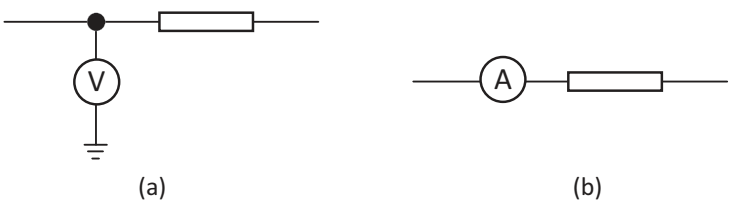

Figure 2.1 Basic measurement instruments: (a) voltmeter; (b) ammeter.

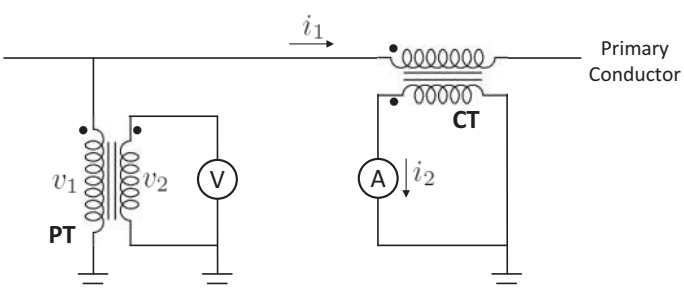

Figure 2.2 Instrument transformers, PT and CT, to measure voltage and current.

where 5 on the right-hand side indicates 5 A, which is the typical reduced current level on the secondary windings. Also, for an ideal PT, we have

$$\frac{v_2}{v_1} = \frac{N_2}{N_1}. \tag{2.2}$$

Some typical turn ratios are 25:1, 60:1, 100:1, and 4500:1. The actual reduced voltage level on the secondary windings may vary for different instruments.

Example 2.1 Suppose a CT with a turn ratio of 100:5 is used to measure current. If the ammeter shows 3.48 A, then the actual current is measured as

$$3.48 \times (100/5) = 69.6 \text{ A}. \tag{2.3}$$

2.1.2 Load Rating and Burden

Instrument transformers often have nameplate parameters for *load rating* and *burden*. The load rating, which is defined mostly for CTs, indicates the maximum load current that can be applied to the primary windings of a CT. That is, for a CT, the load rating is a limit on i_1. In contrast, the burden is associated with the secondary windings of a CT or PT. It indicates the amount of impedance made by the elements of the metering circuit, which may be connected to the secondary windings of the transformer without causing a metering error greater than that specified by its accuracy classification. The burden for each metering device may be indicated in terms of impedance or in terms

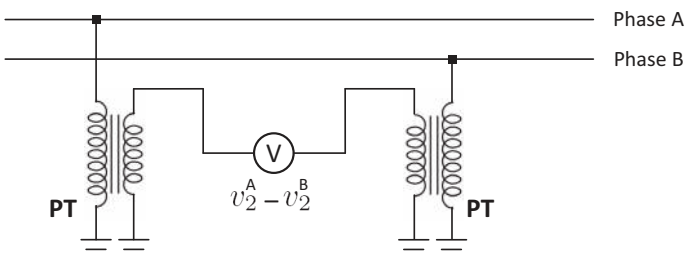

Figure 2.3 Using two identical PTs to measure line-to-line voltage across two phases.

of active and reactive power consumption at a given secondary current and frequency; see Exercise 2.2.

2.1.3 Three-Phase Systems

The setup in Figure 2.2 can be used to connect a PT and a CT to each phase of a three-phase power system to measure voltage and current at each phase.

Voltage in three-phase systems also can be measured across phases. For example, one can use two identical PTs to measure the voltage difference across Phase A and Phase B, as shown in Figure 2.3. Here, the voltmeter measures the *phase-to-phase* voltage, also known as the *line-to-line* voltage. Other possible configurations to use PTs to measure phase-to-phase voltages are explained in [75].

Example 2.2 Suppose two PTs are used to measure line-to-line voltage on a three-phase power system. The turn ratio is 60:1 for both PTs. If the voltmeter shows 206.33 V, then the actual current line-to-line voltage is measured as

$$206.33 \times 60 = 12.38 \text{ kV}. \tag{2.4}$$

2.2 Non-Contact Voltage and Current Sensors

Conventional ammeters and voltmeters are installed as integrated parts of the electric circuit. That is why they need CTs and PTs in order to measure large current and voltage levels. An alternative, more recent approach is to use sensors that measure current and voltage *without* electric contact. Specifically, one can measure the *magnetic field* surrounding a wire to estimate the current that flows through the wire. One can also measure the *electric field* surrounding a wire to estimate the voltage at the wire. The relationships are proportional, between the magnetic field and current and between the electric field and voltage. Non-contact current and voltage sensors are installed on or around *overhead* power lines. A relatively small 42 cm $\times$ 17 cm $\times$ 22 cm line-mounted overhead transmission line sensor, also known as a *bird on wire* sensor, may estimate conductor current up to 1500 A and conductor voltage up to 750 kV [76].

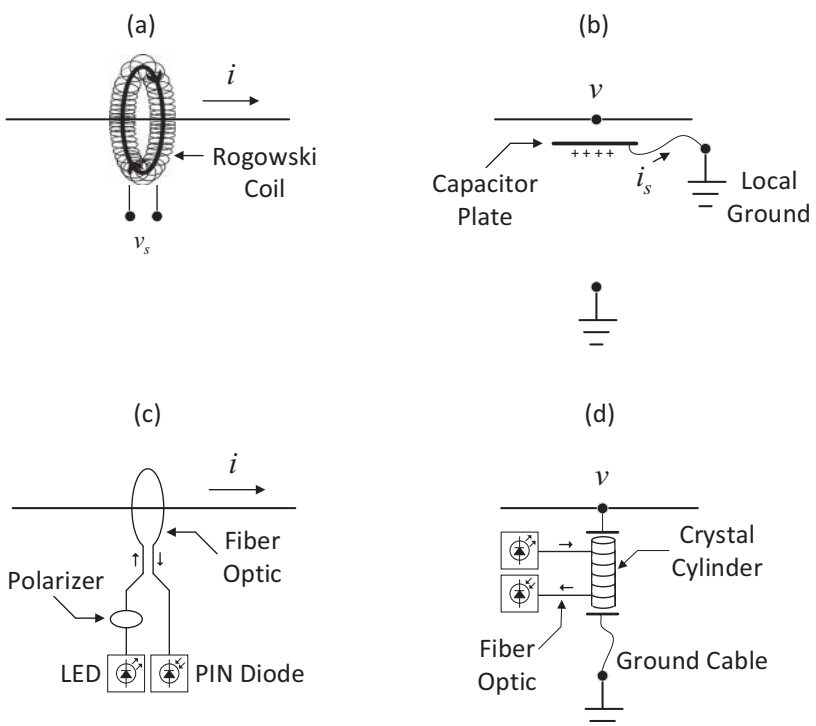

Figure 2.4 Different non-contact overhead line sensor technologies: (a) Rogowski coil to measure current; (b) capacitor plate to measure voltage; (c) magneto-optic transducer to measure current; (d) electro-optic transducer to measure voltage.

2.2.1 Different Working Principles

Different non-contact sensors may use different principles to measure the magnetic and electric fields. For example, in Figure 2.4(a), the current that goes through a conductor is measured by a Rogowski coil that captures the magnetic field surrounding the wire and generates magnetic-field-induced voltage v_s, which is proportional to the rate of change of current. Once this voltage is integrated over time, it provides a signal that is proportional to the current i that goes through the conductor [77]; see Exercise 2.5. In Figure 2.4(b), the voltage between the conductor and the ground is measured by measuring the current i_s between an isolated capacitor plate and a local ground, where the isolated capacitor plate is charged by the electric field surrounding the wire. The measured current is proportional to the voltage v between the conductor and the ground [78].

Another generation of non-contact voltage and current sensors works on principles in *optics*. For example, in Figure 2.4(c), current is measured by a magneto-optic current transducer (MOCT) that exploits the Faraday effect. MOCT detects the impact of the magnetic field surrounding the conductor on rotating the polarization of plane-polarized light that is transmitted by a light-emitting diode (LED) through a single

fiber-optic pass around the conductor. The amount of rotation is proportional to the strength of the magnetic field; thus it is proportional to the current flowing through the conductor [79]; see Exercise 2.4. Also, in Figure 2.4(d), voltage is measured by an electro-optic voltage transducer (EOVT) that exploits the Pockles effect. Here, the full voltage of the conductor is applied between the two end faces of a cylinder-shaped crystal, which has several rounds of fiber-optic winding on its circumferential surface. EOVT detects the impact of the electric field on the optical phase shift in the transmitted light. The detected phase modulation is proportional to the total voltage [80].

2.2.2 Power Harvesting

Most non-contact overhead line sensors are *self-powered*, harvesting power from the conductor's magnetic fields in a non-contact fashion. This is a useful feature because it reduces the need for maintenance and therefore the cost of operation. Power harvesting starts at a minimum *pick-up* conductor current, such as at 12 A on 0.375-inch to 1.030-inch conductors for the line current sensors in [81].

The power-harvesting feature of non-contact sensors may also introduce some new smart grid monitoring applications due to the binary nature of the *sleep* mode (zero) versus the *wake-up* mode (one) caused by their self-powered operation. One such example will be discussed in Section 7.1.2 in Chapter 7.

2.3 Sampling Rate, Reporting Rate, and Accuracy

When addressing power grid modernization, it is natural to focus exclusively on digital sensors, as opposed to the traditional electromechanical meters. Digital sensors are more reliable and provide high measurement accuracy. Two important specifications of digital sensors are the *sampling rate* and the *reporting rate*.

2.3.1 Sampling Rate

The sampling rate of a sensor is indicated in samples per second or samples per cycle of the AC signal. Even if a measured voltage or current signal is purely sinusoidal, its reconstruction requires a minimum sampling rate, namely *twice the frequency of the signal*, according to the Nyquist-Shannon sampling theorem [82]. Proper signal filtering is also needed in order to avoid measurement *aliasing*.

Example 2.3 Consider a sensor that takes eight samples per second. As shown in Figure 2.5, this sensor cannot distinguish a 9 Hz sinusoidal signal from a 1 Hz sinusoidal signal. Hence, a 9 Hz signal may appear to be, i.e., may be aliased to, a 1 Hz signal. From the Nyquist-Shannon sampling theorem, the 8 Hz sampling rate for this sensor allows properly measuring periodic signals with up to $8/2 = 4$ Hz frequency. Therefore, to avoid measurement aliasing, an *anti-aliasing filter*, which is essentially

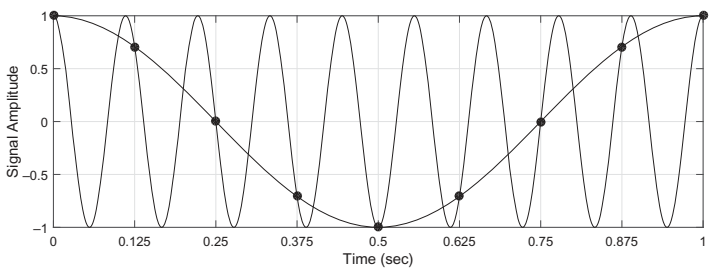

Figure 2.5 An example for aliasing a high-frequency signal to a low-frequency signal.

a low-pass filter, must be placed *before* the signal sampler in order to filter out any measurement signal with a frequency higher than 4 Hz.

More details about anti-aliasing filters are available in [83–86].

2.3.2 Reporting Rate

The reporting rate is the rate at which the sensor reports its measured data. It is often a multiple of the sampling rate to allow pre-processing of the measured data within each reporting interval. As shown in Example 2.4, the reporting rate of a sensor directly affects the type of applications that it can support.

Example 2.4 Consider the RMS readings of the voltage at the secondary of a transformer at a commercial building – one phase only, as shown in Figure 2.6(a). Two voltage sensors are used. One sensor reports 60 readings per second, i.e., it reports one RMS value per AC cycle. The other sensor reports one reading per minute, i.e., it reports the average RMS value of 3600 AC cycles. The data from the low-resolution sensor is sufficient to identify a voltage regulator *tap-changing event* at time 8:37 AM. However, with the use of the higher-resolution sensor, we can zoom in at time 8:45 AM and also identify the *transient response* of a thermostatic load when it switches on, as shown in Figures 2.6(b) and (c). Here, the load switching has caused momentary voltage sag and momentary inrush current. The transient responses take about 100 msec before new steady-state conditions are reached. Such transient responses are *not* visible to the lower-resolution sensor.

Further increasing the reporting rate will introduce another class of sensors that capture the *waveform* of the voltage and current signals; see Chapter 4.

For those sensors where the sampling rate is much higher than the reporting rate, the reported data may include not only the average but also the *minimum* and *maximum* values of the measured quantity. In Example 2.4, the low-resolution sensor may report not only the average RMS value of the 3600 AC cycles, but also the minimum and maximum RMS values across those 3600 AC cycles.

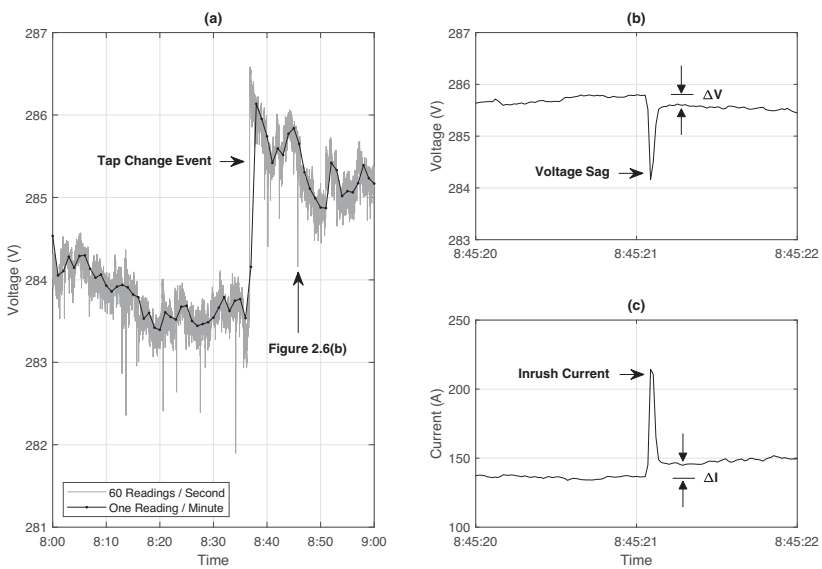

Figure 2.6 (a) An example to compare measuring voltage at two different reading rates; (b) momentary voltage sag; (c) momentary current surge.

2.3.3 Accuracy

The accuracy of a digital voltmeter or ammeter is often given in the form of a percentage of the reading (`rdg`) and/or a percentage of the full scale (`FS`).

Example 2.5 Consider a digital voltmeter with a measurement range of 0 V to 345 V. The accuracy of this voltmeter is $\pm 0.05\%$ `rdg` $\pm\, 0.05\%$ `FS`. If the RMS reading of the voltage is 275 V, then the accuracy of this reading is

$$\pm 0.0005 \times 275 \pm 0.0005 \times 345 = \pm 0.31 \text{ V}. \tag{2.5}$$

If a PT or CT is used, then the accuracy of the measurement depends not only on the accuracy of the measurement device but also on the accuracy of the instrument transformer. For example, the accuracy of a CT is defined based on its rated primary current. For an IEC 60044-1 standard grade, i.e., Class 1.0 CT, accuracy is $\pm 1.0\%$ at 100% of the rated primary current, $\pm 1.5\%$ at 20% of the rated primary current, and $\pm 3.0\%$ at 5% of the rated primary current. Also, a *ratio-correction factor* (RCF) is often defined for CTs as the fraction of the true turn ratio over the nameplate turn ratio. RCF is often provided as a curve plotted against multiples of the rated primary or secondary current for a given constant burden.

Example 2.6 If RCF is 1.01 at a certain primary current for a CT with a nameplate ratio of 100:5, then the true turn ratio is $1.01 \times 100/5 = 20.2$, as opposed to $100/5 = 20$. In other words, the true turn ratio is 100:4.95.

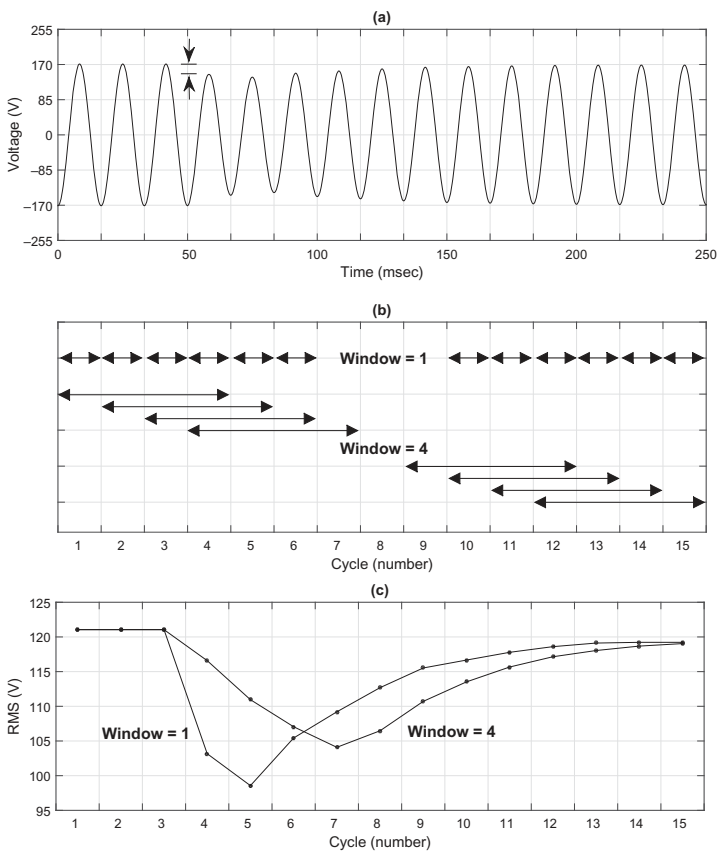

Figure 2.7 The impact of averaging filters: (a) the voltage signal to be measured; (b) measurement windows of lengths one and four cycles; (c) reported RMS voltages.

2.3.4 Impact of Averaging Filters

Most voltage and current sensors use some sort of *averaging filters*; these may include, among others, the low-pass anti-aliasing filter that we discussed in Section 2.3.1. As a result, each individual measurement that is reported by the sensor is the average or weighted average of multiple raw measurements over a finite time interval, known as the *measurement window*. The length of the measurement window varies among sensors and affects their class and performance.

The basic concept of average filtering is illustrated in Figure 2.7. The voltage waveform to be measured is shown in Figure 2.7(a). Two choices of the measurement window are considered: one and four, as shown in Figure 2.7(b). The reporting rate is the *same* in both cases. If the window size is one, then the RMS value of the most recently measured voltage cycle is reported. If the window is four, then the average of the RMS values of the *four most recent* voltage cycles is reported. Accordingly, the transient resolution reported by the sensor is different in each case, as shown in Figure 2.7(c). We can see that the use of averaging filters results in *smoothing* the

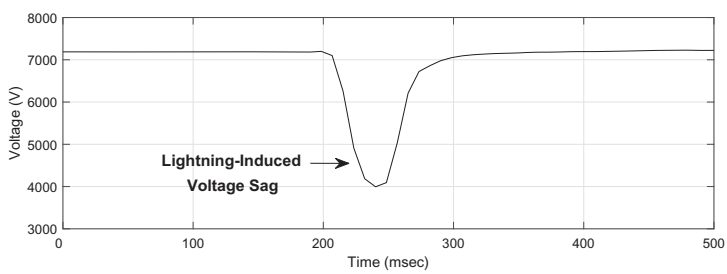

Figure 2.8 A lightning-induced voltage sag, studied in Example 2.7 [87].

measurements. When the measurement window is four, the reported voltage sag is shorter in magnitude and takes longer to settle down.

The details about the averaging filter and other internal mechanisms are often considered proprietary information and not released by sensor manufacturers. Therefore, caution is required when interpreting the measurement data.

Example 2.7 The effect of a lightning strike on a power grid can be traced by monitoring the transient impulse voltages that are induced on the power system. An example is shown in Figure 2.8, where voltage measurements are taken at a power line where the rated voltage is 7200 V. The reporting rate of the sensor is one RMS value per one AC cycle, i.e., 60 readings per second. Based on these measurements, the *lightning-induced voltage sag* lasted about 80 msec. However, it is known that a lightning strike lasts only several microseconds. The discharge of the lightning surge current through a surge arrester also often lasts only a few milliseconds. Therefore, it is likely that the relatively slow response in Figure 2.8 is due to filtering and other internal dynamics of the sensor [87].

The impact of averaging filters is negligible in a steady-state analysis, and even in a dynamic analysis if the transient response is relatively slow compared to the sensor's reporting rate. However, if one tends to analyze very fast events, such as a lightning strike, one may have to use *waveform* sensors; see Chapter 4.

2.4 RMS Voltage and Current Profiles

Traditionally, the voltage and current measurements in the power industry have been mostly in terms of the RMS values of the AC voltage and current waves. This has been particularly the case in the traditional *supervisory control and data acquisition* (SCADA) systems. Therefore, it is important to learn the kinds of analysis that one can do with the RMS voltage and current measurements. For the rest of this chapter, we will focus on the RMS voltage and current measurements. We will discuss measuring voltage and current phasors in Chapter 3 and measuring voltage and current waveforms in Chapter 4, as they require using more advanced sensors.

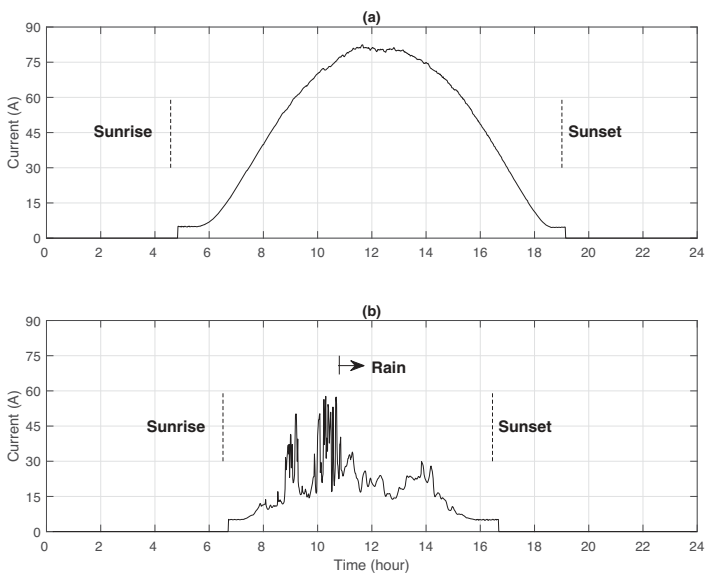

Figure 2.9 Two daily RMS current profiles at a PV inverter's output: (a) a sunny day in summer; (b) a cloudy and rainy day in winter [88].

2.4.1 Daily Profiles

It is often informative to examine the daily RMS profiles of voltage and current, e.g., at a substation, a PV inverter, or a load. In most cases, there is no need for a sensor with a very high reporting rate. A one-minute reporting interval is often sufficient to see the overall trends and to identify the major voltage and current events.

Example 2.8 Two daily profiles of the RMS current measurements that are taken at the output terminals of a solar PV inverter are shown in Figure 2.9. The profile in Figure 2.9(a) is measured on a *sunny* day in *summer*. The profile in Figure 2.9(b) is measured on a *cloudy* and *rainy* day in *winter*. The generation output highly depends on the time of day, season, and weather conditions.

The changes in the current profiles in Example 2.8 are solely due to the changes in solar irradiance at the location of the PV unit. However, when it comes to voltage profiles, the changes and fluctuations can be due to a wide range of causes, as we will see in the next example and its follow-up discussions.

Example 2.9 Figure 2.10 shows the daily RMS profiles of voltage and current measurements at a power distribution feeder [89, 90]. The reporting rate is once per minute. The rated voltage is 7200 V. The RMS voltage profile is relatively stable, remaining between 7050 V, i.e., 0.979 p.u., and 7350 V, i.e., 1.021 p.u. The RMS current profile is generally higher during the day and lower at night. Of interest are

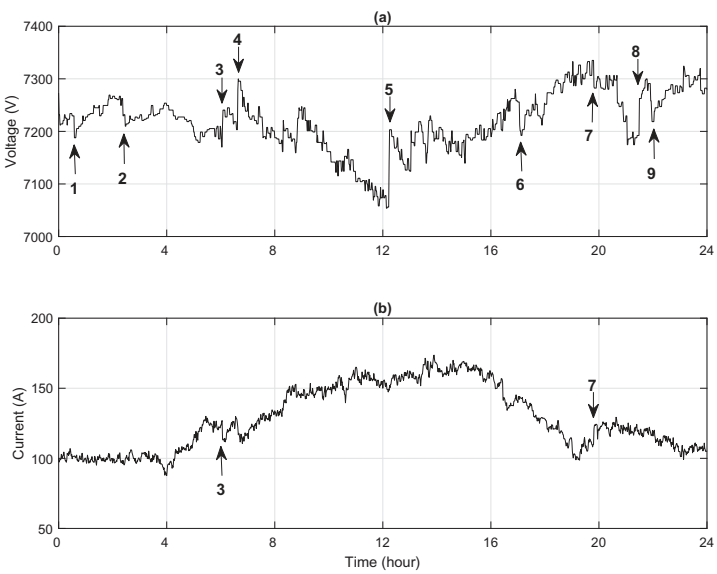

Figure 2.10 Examples of daily RMS profiles – one phase only – at a power distribution feeder: (a) daily voltage profile; (b) daily current profile.

the sudden changes in the RMS voltage profile. A subset of those sudden changes are marked with numbers 1–9. Events 1, 2, 6, 7, and 9 demonstrate voltage sags. Events 3, 4, 5, and 8 demonstrate voltage swells.

The voltage sags and swells that are identified in Example 2.9 are caused by different sources. They could be due to a *local* issue, such as a sudden change in this feeder's load, or the operation of a capacitor bank, a voltage regulator, or another device on this feeder. They could also be due to a *non-local* issue, i.e., a voltage sag or swell that occurred at the substation, sub-transmission system, or transmission system, which also showed up on this feeder's voltage profile.

Events 1, 2, 4, 5, 6, 8, and 9 on the voltage profile are less likely to be due to sudden changes in the feeder's load, because they do *not* coincide with a major change in the current profile. For instance, the current profile is almost flat from midnight until around 3:45 AM, yet there are major changes in the voltage profile in this period, including Events 1 and 2. As for Events 3 and 7, they *do* coincide with some noticeable changes in the current profile, which would be more visible if we zoom in on the figure. Thus, Events 3 and 7 could be *load induced* or caused by other local issues. These two events will be further discussed in Section 5.2 in Chapter 5.

Next, suppose we also obtain the daily RMS voltage profile of a *neighboring* distribution feeder, but under the *same* substation, and on the *same* day. This is shown in Figure 2.11. The reporting rate is again once per minute. The timings of the same nine events that we identified in Example 2.9 are marked and enumerated also in this figure. Events 1, 2, 4, 5, 6, and 9 also showed up quite noticeably in this figure. From

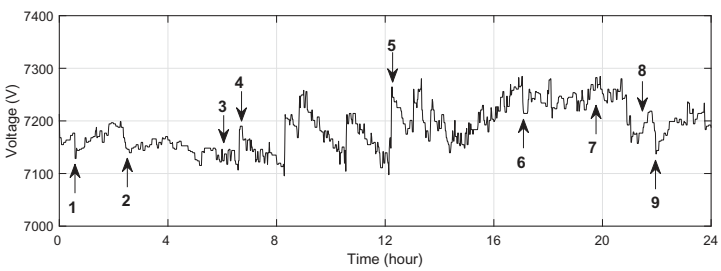

Figure 2.11 Daily RMS voltage profile at a neighboring feeder; compare with Figure 2.10(a). Events 1, 2, 4, 5, 6, and 9 also appear in this feeder's RMS voltage profile.

this, together with the analysis in the previous paragraph, we can conclude that all these events very likely have *root causes* at the substation, sub-transmission system, or transmission system, i.e., they are very likely *not* caused by local issues on either of the two feeders. Similarly, we can now conclude that events 3, 7, and possibly 8 *are* caused by some local issues in the first feeder.

While the above analysis is intuitive and manual, one can use techniques from *statistics* and *machine learning* to extract the above patterns automatically and from large sets of measurement data; see Section 2.7 as well as Section 3.7 in Chapter 3.

2.4.2 Histograms and Scatter Plots

The time period of the daily RMS voltage and current profiles can be extended to several days, weeks, or months. However, for such longer periods, it is often beneficial to present the measurements in a way that can highlight some of their *statistical characteristics*. In this section, we discuss two common options.

Histograms

Histograms can be used to provide an approximate representation of the *distribution* of a large set of measurements. To construct a histogram, we divide the entire range of the measurements into a series of intervals, called *bins*, and we count the number of measurements whose values fall into each interval [91].

Example 2.10 Suppose RMS voltage measurements are available on a minute-by-minute basis at two power distribution feeders for a period of one month. The histogram representation of the measurements at each of these two feeders is shown in Figure 2.12. The range of the measurements is from 6900 V to 7400 V. This range is divided into 25 bins. The first bin includes all the measurements between 6900 V and 6920 V, the second bin includes all the measurements between 6920 V and 6940 V, and so on. The histogram corresponding to Feeder 1 is almost evenly distributed around the rated voltage at 7200 V; see Figure 2.12(a). About 50.5% of the reported voltage measurements are below the rated voltage, and about 49.5% are above the rated voltage. The histogram corresponding to Feeder 2 is wider and placed mostly to

the left of the rated voltage; see Figure 2.12(b). About 85.8% of the reported voltage measurements are below the rated voltage, and about 14.2% are above the rated voltage.

Scatter Plots

The scatter plot corresponding to the minutely voltage measurements in Example 2.10 is shown in Figure 2.13. Here, the voltage measurements at Feeder 2 are plotted *against* their *corresponding* voltage measurements at Feeder 1. Each point represents the measurements at one minute. A total of $60 \times 24 \times 30 = 43,200$ points are shown on this figure. Two key observations are marked on the figure.

First, consider the dashed diagonal line, which is marked as ①. The points *below* this line are associated with the minutes during which the voltage at Feeder 1 was *higher* than the voltage at Feeder 2. This accounts for 90.6% of the points. Conversely,

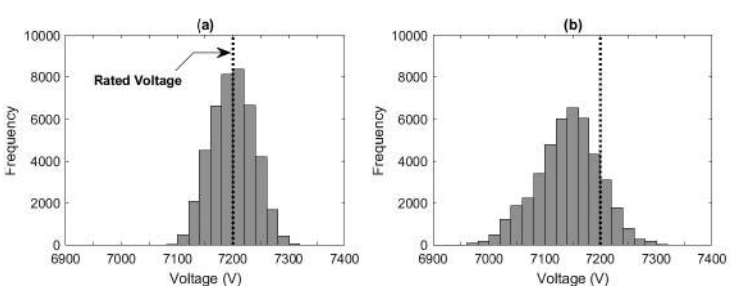

Figure 2.12 The histogram representation of the minutely RMS voltage profiles of two power distribution feeders over one month: (a) Feeder 1; (b) Feeder 2.

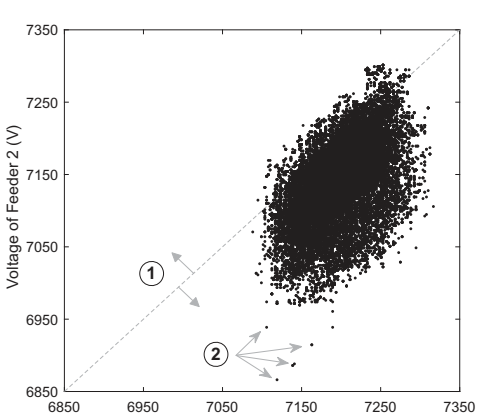

Figure 2.13 Scatter plot corresponding to the voltage measurements in Example 2.10. The diagonal line helps with making comparisons, and the arrows point at the outliers.

the points *above* this line are associated with the minutes during which the voltage at Feeder 1 was *lower* than the voltage at Feeder 2. That accounts for 8.4% of the points. Note that 1.1% of the points are *on* the diagonal line. These are the cases where the voltages were *equal* on both feeders to the extent of the reading resolution of the sensors.

Second, consider the four arrows, which are collectively marked as ②. They point at a few *outliers*. During the minutes associated with these outliers, Feeder 2 experienced unusually major voltage sags that were likely only *local* to Feeder 2 because Feeder 1 did *not* similarly experience such major voltage sags.

Clustering

Scatter plots can sometimes reveal *clusters* of points that can be considered for *classification*, i.e., grouping of measurements that have *similar features*.

Example 2.11 Recall from Example 2.4 in Section 2.3.2 that switching on major loads can cause *inrush current*, which can be captured in the current measurements if the reporting rate of the sensor is sufficiently high. An example is shown in Figure 2.14(a). Here, the inrush current is denoted by ΔI_{inrush}. The change in the *steady-state current* that is due to the increased load is also denoted by ΔI_{steady}. Figure 2.14(b) shows the scatter plot of these two quantities based on all the inrush current cases that were observed at a commercial facility during one day. One immediate observation is related to the outlier case that is marked as ①. More importantly, we can see that the majority of the points in this scatter plot are *clustered* into two groups, which are marked as ② and ③. Note that the points in ③ experience much larger inrush current than the points in ② when compared at the same amount of change in the steady-state current.

We will discuss clustering and classification further in Section 3.7 in Chapter 3, Section 4.3 in Chapter 4, and Section 5.4 in Chapter 5.

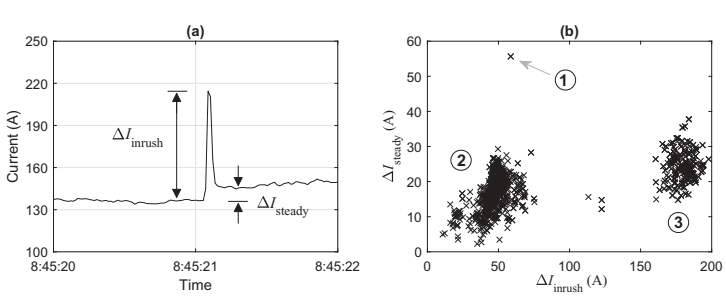

Figure 2.14 Scatter plot for inrush current events: (a) definition of ΔI_{inrush} and ΔI_{steady}; (b) two separate clusters and a few outlier points.

2.5 RMS Voltage and Current Transient Responses

So far we have seen that an event as simple as a load switching, such as the one in Example 2.4, can create a transient response in the power system, at least locally, i.e., at the location where the load switching occurs. Such load-induced transient responses comprise the majority of the (rather minor) transient responses that one can see in voltage and current measurements on an ongoing basis.

However, there are also many other, often more major and more important, causes of transient responses, such as faults and equipment actuations. Their impact usually can be seen more broadly across the power system.

Analysis of transient responses, whether at the load level, the distribution level, or the transmission level, is useful in many power system applications, such as in control, protection, stability analysis, and reliability assessment. The time resolution that is needed depends on the time scale of the transient event being monitored.

2.5.1 Transient Responses Caused by Faults

Example 2.12 The voltage and current transients during an animal-caused fault event at a distribution feeder are shown in Figure 2.15. The fault occurred on a lateral not too far from the substation. Measurements are done on the secondary side of a load transformer at a commercial load location on *another* lateral [92]. Three transient stages are marked by numbers ①, ②, and ③. Stage ① shows the momentary drops in voltage and current during the initial animal-caused short-circuit fault. Stage ②

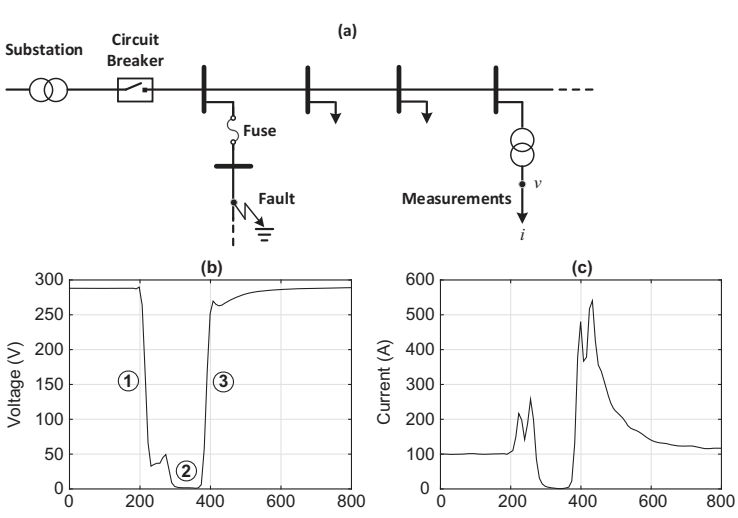

Figure 2.15 (a) One-line diagram of a distribution feeder during an animal-caused fault; (b) voltage readings during the fault; (c) current readings during the fault [92].

shows the momentary power outage (at the location of the sensor) due to the operation of the circuit breaker. Sometime during stages ① and ② the fuse on the faulted lateral burns, isolating the fault. Stage ③ shows the transient in voltage and current after the circuit breaker recloses and restores service.

Impact at Other Locations

Given the significance of the transient response in Example 2.12, one may expect that the fault may have also caused transient responses in other locations on the power grid. That is indeed the case, as we can see in Figure 2.16. The voltage measurements in Figure 2.16(a) are taken at the distribution substation at the *same* distribution feeder. The voltage measurements in Figure 2.16(b) are taken at another substation that is *several miles away* from the faulted location. As we move away from the faulted location, the transient response becomes less significant.

While the animal-induced fault in Example 2.12 caused transient responses in a region that may span tens of miles; there are also other types of more significant disturbances in power systems that may cause transient responses all across the interconnected power grid; that may span hundreds of miles. We will see such system-wide transient responses in Sections 2.6.1 and 2.9.2.

2.5.2 Transient Responses Caused by Equipment Actuations

Example 2.13 A PV farm is interconnected to a power distribution system at a distribution substation. Figure 2.17(a) shows the RMS voltage that is measured at the point of inter-connection. Only one phase is shown here. A major step change is visible, caused by a step-up transformer tap change event in the power system. This voltage event resulted in a *transient response* in the RMS current of the PV farm, as shown in Figure 2.17(b). The pattern of the changes in the RMS current reveals how the inverters at the PV farm respond to the step-up disturbance in voltage; see [93].

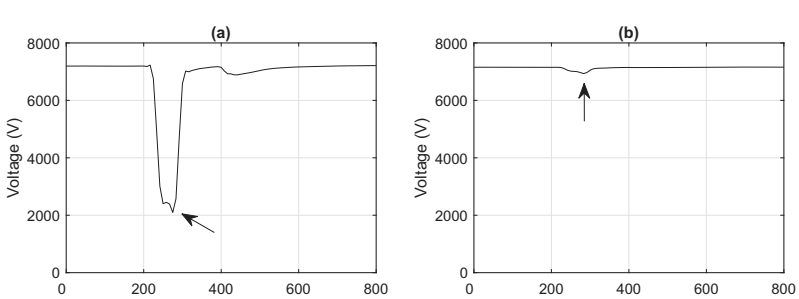

Figure 2.16 Transient responses that are caused by the fault in Figure 2.15 at two other locations: (a) the substation at the same feeder; (b) another substation [92].

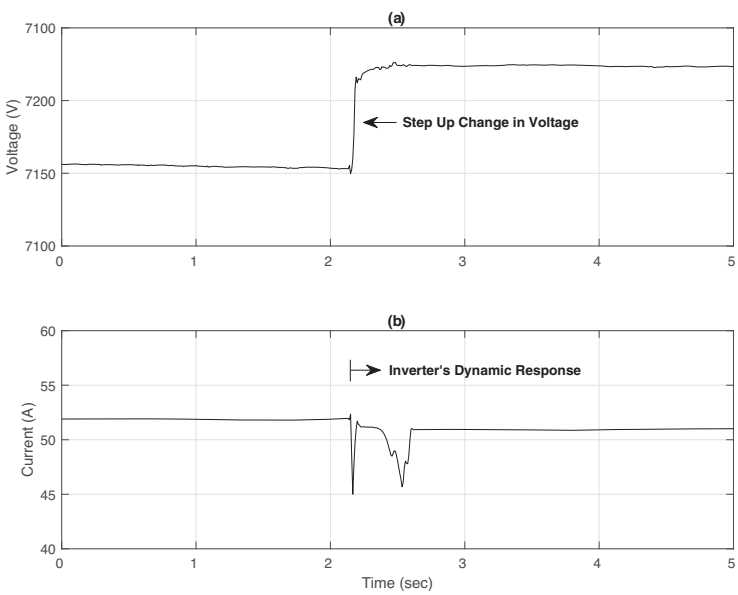

Figure 2.17 Dynamic step response of a PV farm's inverter to a step up voltage event due to a transformer tap change: (a) RMS voltage profile; (b) RMS current profile [93].

The transient response in Figure 2.17(b) takes only about one second. It includes major *undershoots* and a few small *overshoots*. The transient signature in this figure is for the most part a reflection of the dynamics of the inverter control system.

Monitoring the transient responses that are caused by equipment operation can inform us about the *state of the health* of the equipment and the possible signs of *incipient faults* (i.e., early-stage faults) that could become problematic in the future, as well as the overall response of the system under potential contingencies. We will discuss incipient faults in details in Section 4.3 in Chapter 4.

2.6 RMS Voltage and Current Oscillations

Many problems in the power grid begin with or are manifested through *oscillations*. At the transmission level, system-wide oscillations are often associated with the electromechanical dynamics of the power system that are excited by a *disturbance*, such as losing a major power generation unit or losing a transmission line. At the distribution level, local oscillations are often associated with equipment responses to disturbance, circuit resonance, or certain load operations.

Oscillations in power systems are often characterized based on their *oscillatory modes*. If all the oscillatory modes are *stable*, then the oscillations decay and diminish over time. However, if one or more oscillatory modes are *unstable*, then the oscillations grow in magnitude until corrective actions are taken.

In this section, we discuss examples of system-wide and local oscillations that can be seen in voltage and current measurements. We also discuss how to obtain the oscillatory modes of the system from voltage and current measurements.

2.6.1 Wide-Area Oscillations in Power Transmission Systems

System-wide oscillations, also known as *wide-area oscillations*, are common phenomena in power transmission systems. They are caused by the electromechanical oscillations of rotational generators in response to faults in the system, transmission line switching, a sudden change in the output of generators, or a sudden change in major loads. Wide-area oscillations may affect the magnitude, phase angle, and frequency of voltage across the entire interconnected power system.

Some of the common classes of wide-area oscillations include: *local plant mode oscillations*, where one generator swings against the rest of the power system; *inter-area mode oscillations*, where two coherent groups of generators swing against each other, causing excessive power transfers across the network; and *control mode oscillations*, where some generators suffer from poorly tuned exciters, governors, or other generator controllers. These different oscillation modes can sometimes be identified based on the frequency of the oscillations [94]:

- Control mode oscillations: 0.01 Hz to 0.15 Hz;
- Inter-area mode oscillations: 0.15 Hz to 1.0 Hz;
- Local plant mode oscillations: 1.0 Hz to 2.0 Hz.

The above frequency ranges are approximate.

Example 2.14 Figure 2.18 shows the transient inter-area oscillations that were observed in voltage measurements at a 500 kV transmission line after a generation disturbance. The initial disturbance, which is due to losing a major generator unit in the system, resulted in a voltage sag followed by *ring-down* oscillations, i.e., decaying oscillations that ultimately disappear in ambient noise after a few seconds. The dominant mode of oscillations had a frequency of 0.7 Hz.

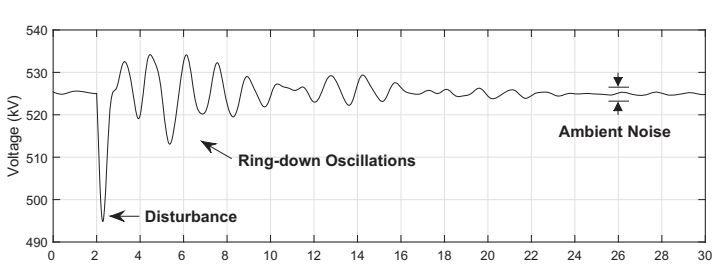

Figure 2.18 Oscillations in voltage at a 500 kV transmission line due to a generation disturbance [95]. The oscillations gradually decay and ultimately disappear in ambient noise.

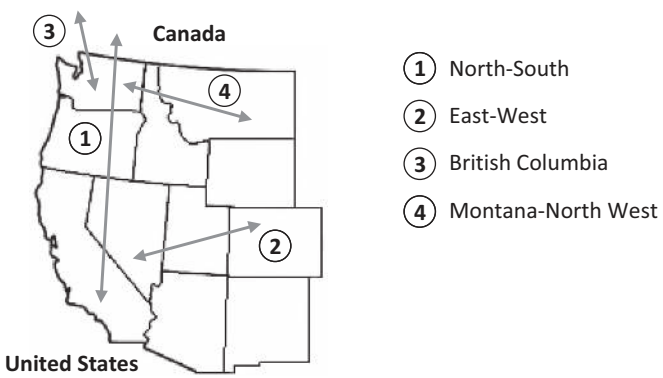

Figure 2.19 The primary modes of inter-area oscillation in the Western Interconnection in the United States. Each mode involves two regions that are connected with an arrow.

Inter-Area Oscillations

Among different types of wide-area oscillations, understanding *inter-area oscillations* is particularly important due to their impact on power system stability and the fact that they involve many parts of the power system in distant regions with complex dynamic behavior. Inter-area oscillations are used in the analysis of power system dynamics because of their relation to small-signal stability [94]. Inter-area oscillations can arise for a variety of reasons, such as excessive power transfers, inefficient damping controls at some generators, or unfavorable load characteristics.

Figure 2.19 shows some of the primary modes of inter-area oscillations in the Western Interconnection in the United States [96]. Each mode involves two geographical regions. For example, the North-South mode involves generators in Canada and the Pacific Northwest region in the United States oscillating against generators in the Desert Southwest and Southern California, causing excessive power swings between Northern California and Oregon as well as between Northern and Southern California. Studies have shown that damping this inter-area oscillation mode can improve system stability and increase the transfer capability of the California Oregon Intertie (COI) corridor on the Western Interconnection; e.g., see [97, 98]. We will discuss inter-area oscillations also in Section 2.9.2, Section 3.4.3 in Chapter 3, and Section 6.4 in Chapter 6.

2.6.2 Local Transient Oscillations in Power Distribution Systems

Some oscillations in power systems are caused by a local issue in the power distribution network, such as due to resonance between a capacitor and an inductor. Such oscillations often affect only the same distribution feeder where the issue occurs. Also, they are likely to be visible only in current measurements, compared to the voltage measurements. As we will see in Chapter 4, some local transient oscillations may

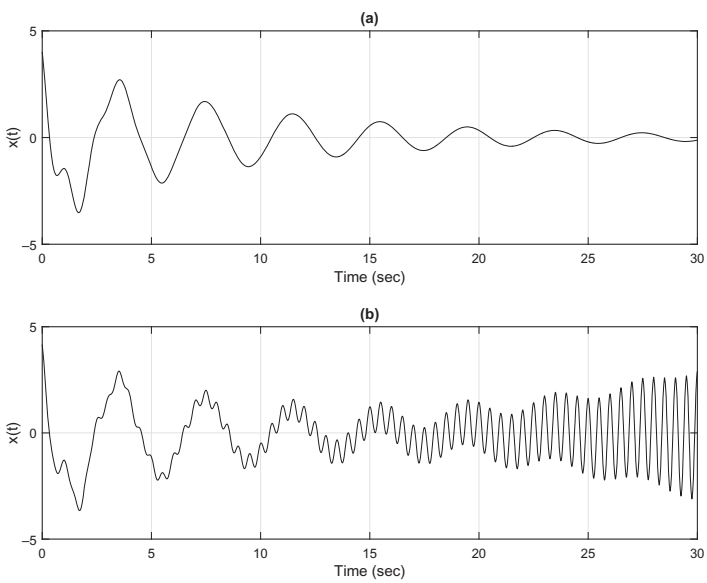

Figure 2.20 Examples of oscillatory modes: (a) stable; (b) unstable.

have very high frequencies at the order of kHz and may last for only a fraction of an AC power system cycle.

2.6.3 Modal Analysis of Oscillations

An oscillatory signal $x(t)$ can be mathematically modeled as

$$x(t) = \sum_{i=1}^{m} A_i e^{\sigma_i t} \cos(w_i t + \varphi_i), \tag{2.6}$$

where m is the number of *oscillatory modes*. For each mode i, notations A_i, φ_i, w_i, and σ_i indicate the *amplitude*, *phase angle*, *angular frequency*, and *damping factor*, respectively. Note that if signal $x(t)$ includes a DC term, then the DC term can be modeled as a mode with zero frequency, a zero damping factor, and a zero phase angle. Signal $x(t)$ can be any *time series*, such as the RMS readings of voltage or current.

Example 2.15 Two oscillatory signals $x_1(t)$ and $x_2(t)$ are shown in Figures 2.20(a) and (b), respectively. Signal $x_1(t)$ has $m = 2$ modes, where $A_1 = 3.5$, $\varphi_1 = \pi/4$, $w_1 = 2\pi \times 0.25$, $\sigma_1 = -0.1$, $A_2 = 1.75$, $\varphi_2 = \pi/6$, $w_2 = 2\pi \times 0.8$, and $\sigma_2 = -0.5$. Both modes are stable and decay over time. Signal $x_2(t)$ has $m = 3$ modes. The first and the second modes are stable and identical to those of signal $x_1(t)$. The parameters of the third mode are $A_3 = 0.15$, $\varphi_3 = 0$, $w_3 = 2\pi \times 2$, and $\sigma_1 = 0.1$. The third

mode is *not* stable, because $\sigma_3 > 0$. As a result, the oscillations corresponding to this mode quickly grow in magnitude.

The model in (2.6) can be represented also in *discrete-time* domain by applying the Z-Transform from digital signal processing [99, 100]. Let Δt denote the reporting interval, i.e., the inverse of the reporting rate, of the sensor; see Section 2.3.2. At each discrete time k, we can model the measurement signal as

$$x(t = \Delta t \times k) = \sum_{i=1}^{m} {z_i}^k R_i, \tag{2.7}$$

where for each mode $i = 1, \ldots, m$, we define:

$$z_i = e^{(\sigma_i + j w_i)\, \Delta t} \tag{2.8}$$

and

$$R_i = A_i e^{j\varphi_i}. \tag{2.9}$$

Since our focus is on digital sensors that report measurements in discrete time, for the rest of this section we use the model in (2.7) instead of (2.6). Also, for notational simplicity, we use $x(k)$ to denote the measurement at discrete time k, instead of the more precise but cumbersome notation $x(t = \Delta t \times k)$.

Prony Method

A popular modal analysis technique is the *Prony method* [101]. It can estimate all four parameters, w_i, σ_i, A_i, and φ_i, for a given measurement signal $x(t)$ based on the discrete-time model in (2.7)–(2.9). This is done in three steps.

First, suppose a total of n measurement points are available, where $n \gg m$. A discrete linear auto-regressive (AR) predictor model is used to capture the dynamics of $x(t)$. In this regard, $x(t)$ at discrete time m is approximated as

$$x(m) = a_1 x(m-1) + a_2 x(m-2) + \ldots + a_m x(0). \tag{2.10}$$

Here we approximate the measurement at discrete time m as a linear combination of all the *previous* measurements at discrete times $m-1, m-2, \ldots, 0$. We can use (2.10) and similarly approximate $x(m+1), x(m+2), \ldots, x(n-1)$; and derive:

$$\begin{bmatrix} x(m) \\ x(m+1) \\ x(m+2) \\ \vdots \\ x(n-1) \end{bmatrix} = \begin{bmatrix} x(m-1) & \cdots & x(0) \\ x(m) & \cdots & x(1) \\ x(m+1) & \cdots & x(2) \\ \vdots & & \vdots \\ x(n-2) & \cdots & x(n-m-1) \end{bmatrix} \begin{bmatrix} a_1 \\ \vdots \\ a_m \end{bmatrix}. \tag{2.11}$$

Let $\mathbf{\Psi}$ denote the $(n-m) \times 1$ vector on the left and $\mathbf{X}$ denote the $(n-m) \times m$ matrix in the middle. Both $\mathbf{\Psi}$ and $\mathbf{X}$ depend solely on measurements. Also, let $\mathbf{a}$ denote the vector of unknown coefficients $a_1, \ldots, a_m$. Since $n \gg m$, we can formulate the

following *least-squares* (LS) optimization problem based on the relationship in (2.11) in order to obtain the unknown coefficients:

$$\min_{\mathbf{a}} \ \|\boldsymbol{\Psi} - \mathbf{X}\mathbf{a}\|_2 \,. \tag{2.12}$$

We can solve the above LS problem by using an LS solver; such as `lsqlin` in MATLAB [102]. Alternatively, we can obtain the solution in closed-form as [103]:

$$\mathbf{a} = (\mathbf{X}^T\mathbf{X})^{-1}\mathbf{X}^T\boldsymbol{\Psi}. \tag{2.13}$$

Second, we use the coefficients $a_1, \ldots, a_m$ that we obtained in the previous step in order to solve the following *discrete-time characteristics polynomial* of degree m, which is associated with the difference equation in (2.10):

$$1 - \sum_{i=1}^{m} a_i z^{-i} = 0. \tag{2.14}$$

After reordering the terms, we have:

$$z^m - \sum_{i=1}^{m} a_i z^{m-i} = \begin{bmatrix} 1 & -\mathbf{a}^T \end{bmatrix} \begin{bmatrix} z^m \\ z^{m-1} \\ z^{m-2} \\ \vdots \\ z \\ 1 \end{bmatrix} = 0. \tag{2.15}$$

We can solve the above equation over unknown z by using a solver such as `roots` in MATLAB [104]. The *roots* (solutions) of the discrete-time characteristics polynomial provide the *poles* corresponding to the oscillatory modes of the measured signal. Such poles are in the discrete-time domain. From (2.8), we can derive:

$$\sigma_i + jw_i = \ln(z_i)/\Delta t, \quad i = 1, \ldots, m. \tag{2.16}$$

By applying the definition of complex logarithm, we can rewrite (2.16) as

$$\sigma_i = \ln\left(|z_i|\right)/\Delta t, \ \ w_i = \angle z_i/\Delta t, \quad i = 1, \ldots, m. \tag{2.17}$$

Third, once z_i is known for all $i = 1, \ldots, m$, we can use (2.7) to construct:

$$\begin{bmatrix} x(0) \\ x(1) \\ x(2) \\ \vdots \\ x(n-1) \end{bmatrix} = \begin{bmatrix} 1 & \cdots & 1 \\ z_1 & \cdots & z_m \\ z_1^2 & \cdots & z_m^2 \\ \vdots & & \vdots \\ z_1^{n-1} & \cdots & z_m^{n-1} \end{bmatrix} \begin{bmatrix} R_1 \\ \vdots \\ R_m \end{bmatrix}. \tag{2.18}$$

Let $\boldsymbol{\Phi}$ denote the $n \times 1$ vector on the left and $\mathbf{Z}$ denote the $n \times m$ matrix in the middle. Vector $\boldsymbol{\Phi}$ depends solely on measurements. Matrix $\mathbf{Z}$ is the solution of the discrete-time characteristics polynomial in (2.15) that we obtained in the second step. Therefore, both $\boldsymbol{\Phi}$ and $\mathbf{Z}$ are known. Also, let $\mathbf{R}$ denote the vector of unknown residues

Table 2.1 Oscillation modes obtained in Example 2.16

Mode	Frequency (Hz)	Damping (Hz)	Amplitude (kV)	Phase Angle (°)
1	± 1.6056	−0.9081	5.0083	±45.419
2	± 1.5002	−0.2515	1.1597	∓74.344
3	± 1.2395	−0.3032	2.2171	±55.979
4	± 1.0872	−0.4831	2.2250	±45.605
5	± 0.7241	−0.0767	2.3696	±30.464
6	± 0.6540	−0.1128	3.0296	±105.92
7	± 0.2890	−0.3598	4.6563	±162.87

$R_1, \ldots, R_m$. We can formulate an LS optimization problem similar to the one in (2.12) and obtain its solution as

$$\mathbf{R} = (\mathbf{Z}^T\mathbf{Z})^{-1}\mathbf{Z}^T\mathbf{\Phi}. \tag{2.19}$$

Given the above solution for $\mathbf{R}$, we can use (2.9) to obtain:

$$A_i = |R_i|, \quad \varphi_i = \angle R_i, \quad i = 1, \ldots, m. \tag{2.20}$$

Once all the m oscillatory modes are calculated, one may still need to do some post-processing before the results can be used. For example, it is known that the Prony method usually results in *aliased modes* [105]. In fact, based on an analysis similar to that in Section 2.3.1, we can show that any oscillatory mode with a frequency that is higher than half the reporting rate of the sensor is prone to aliasing. Such oscillatory modes are not reliable and should be discarded from the results.

Example 2.16 Again, consider the ring-down oscillations in the voltage measurements in Figure 2.18 in Example 2.14. The reporting interval for the measurements is $\Delta t = 0.1$ second. By choosing $m = 101$, the Prony method results in calculating 101 oscillatory modes. A total of 86 modes have frequencies higher than $0.5/0.1 = 5$ Hz. Thus, they are prone to aliasing and are discarded. The remaining 15 modes include one DC mode with an amplitude of 524.19 kV and seven pairs of complex conjugate oscillatory modes, as listed in Table 2.1.

The modes that we identified in Example 2.16 are shown in Figure 2.21. The DC mode is shown in Figure 2.21(a). The seven oscillatory modes are shown in Figures 2.21(b)–(h). All modes are plotted starting at time $t = 2$ seconds, which is the moment when the disturbance occurs, which is the start of the oscillations

When combined, that is, when they are added together, the above 15 modes provide a Prony estimation for the original measurements in Figure 2.18. The Prony estimation and the original measurements are compared in Figure 2.22. We can see that the Prony estimation is particularly accurate during the first few seconds and then gradually drifts from the measurements. Accuracy of the Prony estimation may increase by increasing the parameter m; see Exercise 2.17.

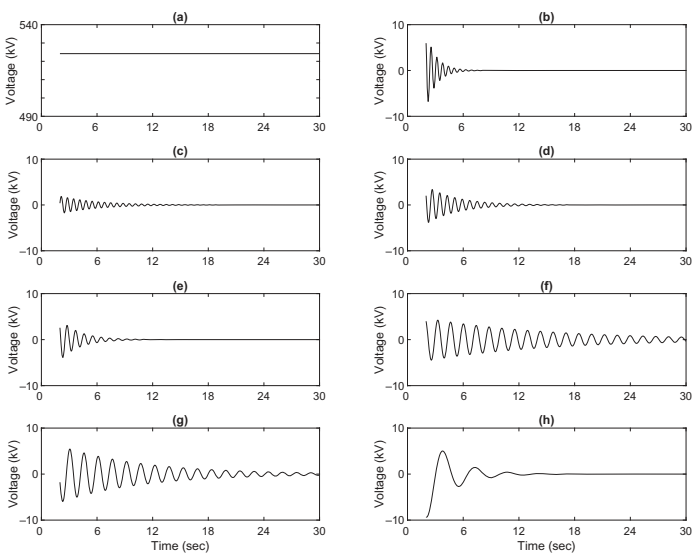

Figure 2.21 All the modes that were obtained by using the Prony method in Example 2.16: (a) DC mode; (b)–(h) complex conjugate oscillatory modes as listed in Table 2.1.

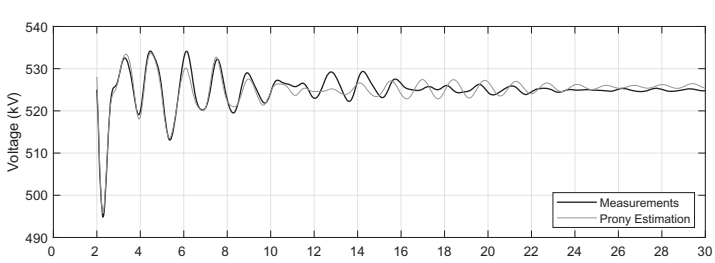

Figure 2.22 Comparing the Prony estimation with the original measurements in Example 2.16. The Prony estimation is the summation of all the modes in Figure 2.21.

The Prony method has been widely studied for the analysis of oscillatory modes in different types of measurements in power systems. Adjustments, improvements, and alternative methods have been proposed in the literature, such as in [106–113].

Fourier Method

Prony analysis is an extension of the well-known *Fourier analysis*. Prony analysis forms a sum of damped sinusoidal terms. In contrast, Fourier analysis forms a sum of sustained sinusoidal terms, where the damping factor is zero at all frequencies. In this regard, we can still use the Fourier Transform (FT) or Fast Fourier Transform (FFT) as a quick method to estimate only the frequency, not the damping factor, of the oscillatory modes in the measurements. The FFT of the measurements can be obtained by using the command `fft` in MATLAB [114].

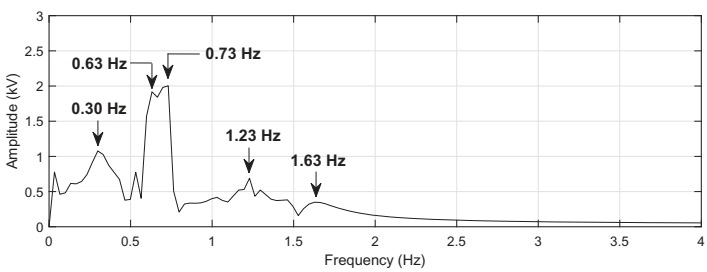

Figure 2.23 Frequency spectrum of the voltage measurements in Example 2.16.

The frequency spectrum of the voltage measurements in Example 2.16 is shown in Figure 2.23. The frequencies that are marked on this figure are comparable with those in Table 2.1. In particular, the frequency modes at 0.30 Hz, 0.63 Hz, 0.73 Hz, 1.23, Hz, and 1.63 Hz in Figure 2.23 more or less match the frequency modes in rows 7, 6, 5, 3, and 1 in Table 2.1, respectively. These are the primary modes of oscillations that an FFT analysis can identify relatively quickly.

Since FFT is computationally less complex than the Prony analysis, it is often used to *detect* oscillations; e.g., see Example 2.35. Once detected, the oscillation can be characterized using the Prony method.

2.7 Events in RMS Voltage and Current Measurements

Events in power systems can be defined broadly as any *change* in any component in the system that is *worth studying*. Events may include major faults and equipment failures that can affect stability and reliability of the system. We saw instances of such events in Examples 2.12 and 2.14. Events may also include load switching or transformer tap changing actions that are *benign* yet may reveal some useful information about the power system and its components. We saw instances of such events in Examples 2.11 and 2.13.

Of course, whether or not an event is "worth studying" depends on what we are trying to achieve in our study. An event could be of great importance for one smart grid monitoring purpose but useless for another smart grid monitoring purpose. For example, when our goal is to study inter-area oscillations at the Western Interconnection, the oscillations in the frequency of the voltage measurements are a critical event to study, as we will see in Section 2.9.2; but an animal-caused fault at a distribution line, such as what we saw in Figure 2.15, is just a small noise in the analysis of system-wide oscillations. In contrast, when our goal is to study the operation of the protection system at a distribution feeder, the animal-caused fault is a key event; but the fluctuations in the voltage frequency due to inter-area oscillations are of no interest.

The definition of events in a study may also depend on the type of sensors that are used and their characteristics. For example, some events could last for only a very short period of time; therefore, they may not be captured by our sensor, depending on

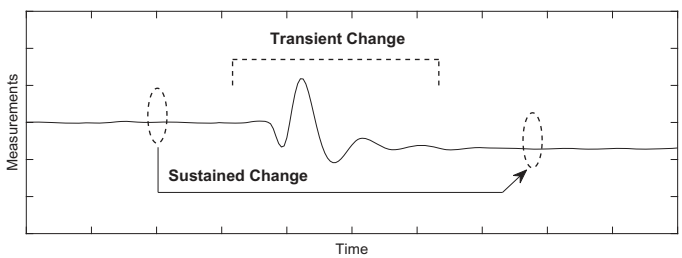

Figure 2.24 An event can show up in the voltage and/or current measurements in form of major transient changes, a major sustained change, or both.

the sampling rate and the reporting rate of the sensor. Furthermore, some events may not manifest in the typical RMS voltage and RMS current measurements, but they do show up if we have access to the phase angle measurements of the voltage and current phasors (see Chapter 3), or the actual waveform measurements of voltage and current (see Chapter 4).

2.7.1 Transient Events versus Sustained Events

Despite the complexities around the definition of events, we can still define two types of events that can help us with the analysis of events throughout this book, namely *transient* events and *sustained* events. The basis for this classification is shown in Figure 2.24. If the event causes a significant transient change in the measurements, then the event is a transient event, and the transient change is likely worth studying. If the event causes a significant sustained change, then the event is a sustained event, and the sustained change is likely worth studying. Note that if an event causes *both* significant transient changes and significant sustained changes, then it could be considered both a transient event and a sustained event, depending on the purpose of our analysis.

The generation disturbance in Example 2.14 caused a major voltage sag and several cycles of oscillations in the voltage measurements, as we saw in Figure 2.18; but as soon as the transient response disappeared, the voltage returned to the same level as it was prior to the event. Therefore, we can consider this event as a transient event as far as the voltage measurements in Figure 2.18 are concerned.

The transformer tap changing event in Example 2.13 in Section 2.5.2 caused a significant sustained change in the voltage measurements in Figure 2.17(a); however, it did *not* cause any major transient response in the voltage measurements in this figure. Therefore, we can consider this event as a sustained event as far as the voltage measurements in Figure 2.17(a) are concerned. As for the same event that is also seen in the current measurements in Figure 2.17(b), it has caused considerable sustained changes as well as significant transient changes. Therefore, we might consider this event as both a sustained event and a transient event as far as the current measurements in Figure 2.17(b) are concerned.

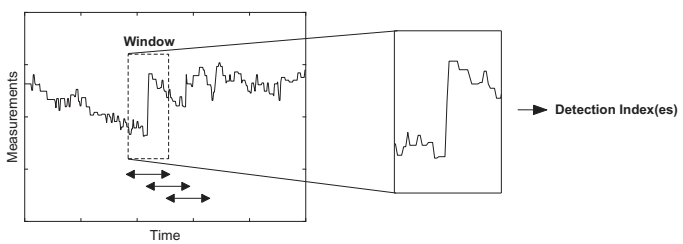

Figure 2.25 Event detection based on calculating a detection index over a window of measurements. The window moves forward in time to detect more events.

2.7.2 Event Detection Methods

In this section we discuss some basic methods to detect events in voltage and current measurements. All these methods include the following three steps:

1. A window of measurements is considered;
2. One or more indexes are calculated based on the window of measurements;
3. An event is detected if the index(es) exceed certain threshold(s).

The window then moves forward in time, and the above three steps are repeated in order to continue detecting more events; see Figure 2.25.

Min-Max

A simple detection index is the difference between the maximum and the minimum values within the window of measurements [113]. Let us define

$$\text{Min-Max Index} = \max\{x_w(t)\} - \min\{x_w(t)\}. \tag{2.21}$$

where $x_w(t)$ denotes the measurements within a given window w. An event is detected in window w if the Min-Max Index exceeds a predetermined threshold.

Example 2.17 Consider the daily voltage profile in Example 2.9 in Section 2.4. Recall that the measurements are reported on a minutely basis. Suppose we set the window size to 20 minutes, i.e., to include 20 measurement points. Thus, the day is divided into $24 \times 60/20 = 72$ windows. Note that, in this example, we assume that the measurement windows do *not* overlap. Figure 2.26 shows the Min-Max Index that is calculated for each of the 72 windows. Suppose we set the detection threshold to 70 kV. Therefore, a window of measurements is deemed to contain an event if the difference between the maximum reported voltage and the minimum reported voltage within the window is at least 70 kV. This results in detecting eight events. Five of them are among the events that we had previously marked in Example 2.9, labeled as 3, 4, 5, 8, and 9. They are positioned *above* the threshold curve. Importantly, four of the events that we had marked in Example 2.9 are *not* detected here, labeled as 1, 2, 6, and 7. They are positioned *below* the threshold curve.

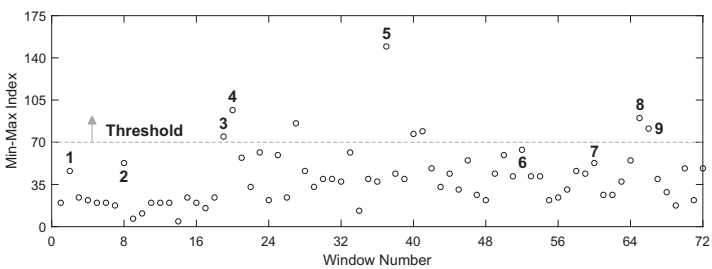

Figure 2.26 Using the Min-Max method to detect the events in voltage measurements in Example 2.17. The numbers refer to the labels of the events in Example 2.9.

The results in Example 2.17 are sensitive to the choice of the threshold. For instance, if we reduce the threshold from 70 kW to 40 kW, the total number of windows that are detected to contain events would increase from 8 to 31; and all of the nine events that we had previously marked in Example 2.9 would be detected. The caveat is that more windows with normal operation would fall in the event category.

Median Absolute Deviation

Detection indexes also can be defined based on principles in statistics. Here, we discuss one such index. Let use define the *median absolute deviation* as

$$\text{MAD} = \gamma \text{ Median} \left\{ \left| x_w(t) - \text{Median}\{x_w(t)\} \right| \right\}. \tag{2.22}$$

A typical value for coefficient γ is 1.4826 [115]. An event is detected in window w if *any* of the measurements within window w is *lower* than

$$\text{Median}\{x_w(t)\} - \zeta \text{MAD}; \tag{2.23}$$

or if *any* of the measurements within window w is *higher* than

$$\text{Median}\{x_w(t)\} + \zeta \text{MAD}. \tag{2.24}$$

A typical value for coefficient ζ is 3. Next, we define:

$$\text{MAD-Low Index} = \min\{x_w(t)\} - (\text{Median}\{x_w(t)\} - \zeta \text{MAD}) \tag{2.25}$$

and

$$\text{MAD-High Index} = \max\{x_w(t)\} - (\text{Median}\{x_w(t)\} + \zeta \text{MAD}). \tag{2.26}$$

An event is detected in window w if the MAD-Low Index is less than zero *or* the MAD-High Index is greater than zero. The former indicates the presence of an *undershoot* among the measurements in window w, while the latter indicates the presence of an *overshoot* among the measurements in window w.

Example 2.18 Again, consider the daily voltage profile in Example 2.9 in Section 2.4. As in Example 2.17, suppose the window size is 20. Figure 2.27(a) shows a window of measurements where an event is detected, because part of the measurements appears

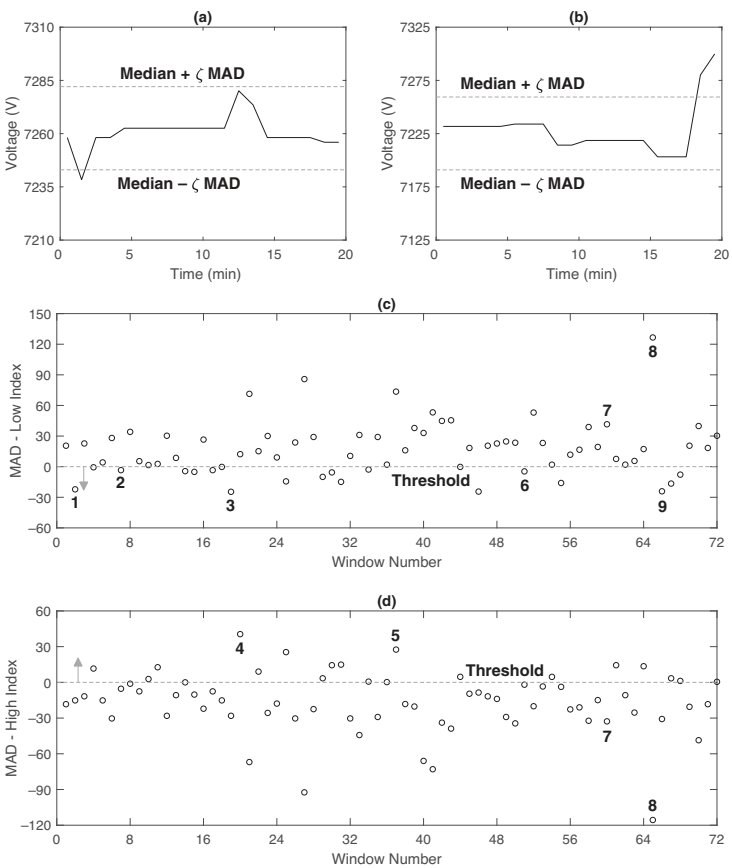

Figure 2.27 Using the MAD method to detect the events in voltage measurements in Example 2.18: (a) and (b) windows with events that are detected due to an undershoot and an overshoot, respectively; (c) and (d) MAD-Low Index and MAD-High Index across all 72 windows, respectively. The numbers refer to the labels of the events in Example 2.9.

below the threshold in (2.23). Figure 2.27(b) shows a window of measurements where an event is detected, because part of the measurements appears *above* the threshold in (2.24). Figures 2.27(c) and (d) show the MAD-Low Index and the MAD-High Index calculated for each of the 72 windows, respectively. Seven of the events that we had previously marked in Example 2.9 are detected, labeled as 1, 2, 3, 4, 5, 6, and 9. Event 8 is not detected; however, this event *can* be detected once we use *partially overlapping windows*, as we will discuss at the end of this section. Event 7 cannot be detected, even with partially overlapping windows, unless we reduce parameter ζ, which may result in detecting too many cases as events. To understand why the situation with Event 7 is different, recall from Example 2.9 that Event 7 is likely caused by a local issue in the distribution network. Therefore, the voltage measurements may not be the best indicator if our goal is to detect local events such

as Event 7. In such cases, it is better also to check the current measurements, as we saw in Figure 2.10(b), in order to search for potential locally events.

Fast Fourier Transform

The Min-Max and MAD methods are usually effective in detecting major sustained events as well as transient events that involve major impulses. However, when it comes to transient events that involve oscillations, it might be better to use *frequency spectral* methods to detect such events. A common frequency spectral method is FFT. In this method, FFT is applied to each window of voltage or current measurements in order to obtain the frequency spectrum associated with the measurements in that window. An event is detected if the amplitude of any frequency component in the frequency spectrum exceeds a predetermined threshold.

Figure 2.28(a) shows the voltage measurements during the oscillatory event that we previously saw in Example 2.14 in Section 2.6.1. Figure 2.28(b) shows the corresponding frequency spectrum that is obtained by applying FFT to the window of measurements in Figure 2.28(a). If we set the event detection threshold to 1.5 kV, then this oscillatory event is detected because the frequency spectrum exceeds the threshold around the 0.63 Hz–0.73 Hz frequency range.

Other Detection Methods

There exist several other event detection methods that can be used to detect events in voltage and current measurements. Some of these methods can be seen as variations or extensions of the methods that we discussed above. For example, one can use *mean* instead of *median* in the MAD method. There are also many options among the frequency spectral event detection methods, such as the Yule-Walker method [113] and the Wavelet method [116, 117].

Some recent methods also use machine learning in both *supervised* and *unsupervised* settings. In supervised event detection, prior knowledge is used to identify and characterize the common patterns for the kind of events that we are interested in detecting. The event detection algorithm then looks for those specific patterns in order to detect the intended events; see the methods in [118–122]. In unsupervised event

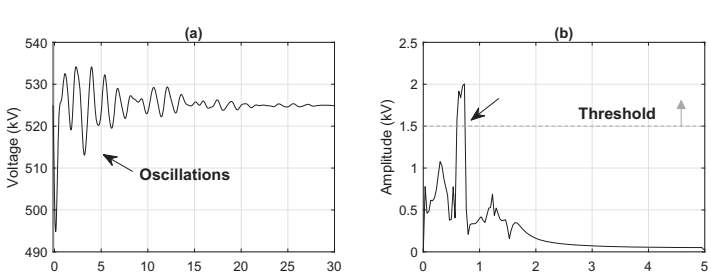

Figure 2.28 Using the FFT method to detect an oscillatory event: (a) a window of voltage measurements; (b) the corresponding frequency spectrum.

detection, no prior knowledge is used. Instead, the goal is to learn the *normal* trends in measurements and then detect an event whenever there is an *abnormality*, i.e., a major deviation from the identified normal trends; see the methods in [123–126].

Overlapping Windows and Dynamic Windows

It is very common in event detection to use windows that have some *overlap* with each other. Such overlap can help avoid missing the events that may fall on the borderline of two adjacent but non-overlapping windows. For instance, in Example 2.18, we did not detect Event 8 because it appeared partially in one window and partially in another window. However, once we use a sequence of windows with 50% overlap, i.e., each window overlaps with half of the previous window and also with half of the next window, we are able to detect this event.

Sometimes it may help to also use *dynamic* windows. For example, if no event is detected in a window of measurements, then we can try *increasing* or *decreasing* the window size before we conclude that there is indeed no event in the considered window of measurements. Using dynamic windows might be a necessity if we expect the events to have different lengths in time; e.g., see [127].

2.7.3 Events in Other Types of Measurements

The focus in this Chapter has been on events in RMS voltage and RMS current measurements. However, events can be of interest in any type of smart grid measurements. We will discuss events in voltage and current phasor measurements in Section 3.7 in Chapter 3, events in voltage and current waveform measurements in Section 4.4 in Chapter 4, and events in active and reactive power measurements and power factor measurements in Section 5.2.1 in Chapter 5.

2.8 Three-Phase Voltage and Current Measurements

A power grid is a three-phase power system. Since the three phases are often *balanced* at the transmission level, it might be sufficient to measure voltage and current on only one phase when we monitor the operation of the power transmission system. However, when it comes to monitoring the power distribution system, the three phases are often *unbalanced* due to the unbalanced distribution of loads, or even due to an unbalanced power distribution grid topology. Therefore, it is often necessary to monitor all three phases in power distribution networks, including at load locations.

2.8.1 Three-Phase RMS Profiles

Figures 2.29(a) and (b) show the RMS voltage and RMS current profiles at each phase of a three-phase load. We can see that the power system is *not balanced*, as the RMS

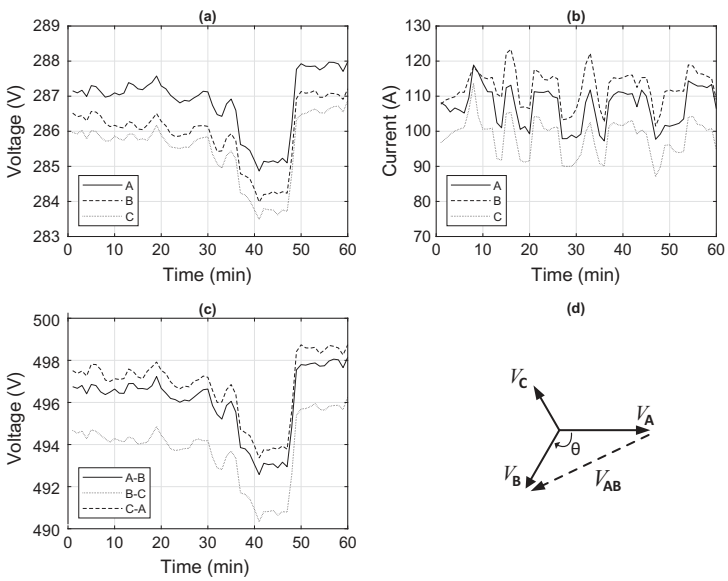

Figure 2.29 Three-phase measurements: (a) voltage; (b) current; (c) line-to-line voltage; (d) relationship between line-to-line voltage and phase voltages.

voltage and current profiles are not identical across the three phases. However, the RMS profiles do generally resemble each other in this example.

Figure 2.29(c) also shows the RMS profile for the line-to-line voltage that is measured at the same three-phase load. By comparing the line-to-line voltage measurements in Figure 2.29(c) with the phase voltage measurements in Figure 2.29(a), we can see that the RMS voltage profiles generally look similar; however, there are advantages in measuring both phase voltages and line-to-line voltages. For example, as shown in Figure 2.29(d), we can use the measurements for line-to-line voltage V_{AB} and the measurements for phase voltages V_A and V_B to obtain the *angle* between voltage *phasors* at Phase A and Phase B, as follows:

$$\cos(\theta) = \frac{{V_A}^2 + {V_B}^2 - {V_{AB}}^2}{2\, V_A\, V_B}. \tag{2.27}$$

Example 2.19 Suppose RMS voltage at Phases A and B is measured as

$$\begin{aligned} V_A &= 286.63\ V \\ V_B &= 287.26\ V. \end{aligned} \tag{2.28}$$

And the RMS line-to-line voltage across Phases A and B is measured as

$$V_{AB} = 497.70\ V. \tag{2.29}$$

From (2.27), we obtain $\cos(\theta) = -0.5042$. Therefore, we have $\theta = -120.28^\circ$.

We will discuss voltage and current phasor measurements in Chapter 3.

2.8.2 Measuring Phase Unbalance

If the voltages in a three-phase power system are not balanced, then some equipment, mainly induction motors, can perform poorly. Therefore, we may need to assess the extent of unbalance in voltage measurements using a suitable index. For instance, the National Equipment Manufacturers Association (NEMA) has introduced Percentage Unbalance (PU) as a metric as follows [128]:

$$\text{PU} = \frac{1}{\Gamma} \max \left\{ |V_{AB} - \Gamma|, |V_{BC} - \Gamma|, |V_{CA} - \Gamma| \right\} \times 100\%, \tag{2.30}$$

where

$$\Gamma = \frac{1}{3} (V_{AB} + V_{BC} + V_{CA}) \tag{2.31}$$

denotes the line-to-line voltage average. Most motors allow a 1% voltage unbalance without derating. However, 2%, 3%, 4%, and 5% voltage unbalance can result in a 0.95, 0.88, 0.82, and 0.5 Derating Factor (DF), respectively [129]. The ANSI C84.1 standard states that utilities should limit their voltage unbalance to 3%.

Example 2.20 Suppose line-to-line voltages are measured at a load as

$$\begin{aligned} V_{AB} &= 497.70\ V \\ V_{BC} &= 494.87\ V \\ V_{CA} &= 496.98\ V. \end{aligned} \tag{2.32}$$

From (2.30) and (2.31), we can obtain

$$\text{PU} = \frac{1.6467}{496.52} \times 100\% = 0.33\%. \tag{2.33}$$

Since PU $< 1\%$, such voltage unbalance does not cause derating in motor loads.

2.8.3 Phase Identification

Electric utilities often do not have reliable records about how the three phases of each distribution feeder are connected to the loads. Even if phase connections are initially recorded correctly, they may change over time due to service restoration, topology reconfiguration, or repairs. Wrong phase labeling is a major source of error in the analysis of power distribution systems. Therefore, it is critical to use available sensor data to correctly identify the loads on each phase.

The basic idea in the phase identification problem is illustrated in Figure 2.30. The feeder serves several loads, including a single-phase load at load point 1 and a three-phase load at load points 2, 3, and 4, as shown in Figure 2.30(a). There are three possibilities for the connection of the single-phase load, as shown in Figure 2.30(b). There are also six possibilities for the connection of the three-phase load, as shown in Figure 2.30(c). The phase identification problem is the problem of identifying the correct phase connection configuration at each load.

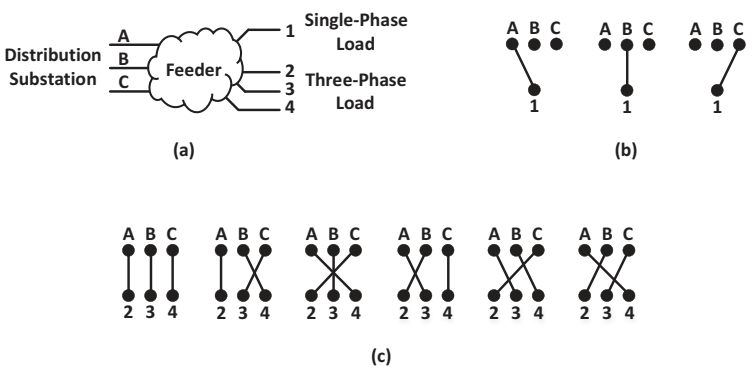

Figure 2.30 The phase identification problem: (a) phase connections are unknown at load points 1, 2, 3, 4; (b) there are three possibilities for the connection of the single-phase load; (c) there are six possibilities for the connection of the three-phase load.

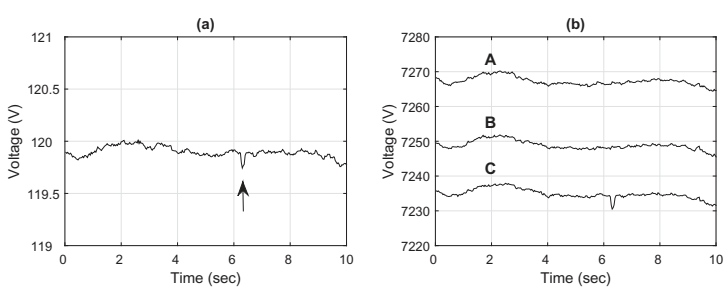

Figure 2.31 Phase identification by comparing voltage profiles: (a) voltage profile at a single-phase load; (b) voltage profiles on three phases at the feeder head at the substation.

Example 2.21 Consider the voltage measurements at a single-phase load as shown in Figure 2.31(a). Suppose the phase connection is unknown for this load. The voltage measurements on three phases at the substation are shown in Figure 2.31(b). They are labeled as Phases A, B, and C. By comparing the voltage profile in Figure 2.31(a) with each of the three voltage profiles in Figure 2.31(b), it is clear that the single-phase load is connected to Phase C. Specifically, the *sudden momentary voltage sag* that is marked in Figure 2.31(a) is seen *only* in Phase C in Figure 2.31(b). All the measurements in this example are reported at 30 readings per second.

The phase identification method in Example 2.21 can also be discussed in the context of the event analysis in Section 2.7. That is, we identified the phase connection by detecting an event on the single-phase measurements in Figure 2.31(a) and comparing it with an event that we detected at the same window on Phase C of the three-phase measurements in Figure 2.31(b), while considering the fact that no similar event was detected at this window on Phase A and Phase B.

Another note about the phase identification method in Example 2.21 is that it is applicable only if the voltage measurements are reported at high rates. If we reduce the reporting rate from 30 readings per second to 1 reading per second, then we cannot detect the event that helped us identify the phase connections based on the voltage profiles in Figure 2.31. However, we can still use some statistical methods to solve the phase identification problem even at lower reporting rates; e.g., see [130, 131].

One statistical measure that can be used for phase identification is the *correlation coefficient* between the voltage measurements at the unknown phase and the voltage measurements at each of the three known reference phases. For example, the correlation coefficient between V_1 and V_A can be obtained as

$$\text{Corr}\,(V_1, V_A) = \frac{\text{Cov}\,(V_1, V_A)}{\sqrt{\text{Var}\,(V_1)\,\text{Var}\,(V_A)}}, \tag{2.34}$$

where $\text{Cov}(\cdot,\cdot)$ and $\text{Var}(\cdot)$ denote the co-variance and variance operators, respectively [91]. We can similarly obtain $\text{Corr}\,(V_1, V_B)$ and $\text{Corr}\,(V_1, V_C)$. A higher correlation coefficient indicates *stronger correlation* between the two voltage profiles, suggesting that the measurements are done at the same phase of the circuit.

Example 2.22 Again, consider the phase identification problem in Example 2.21. Suppose all the voltage measurements are reported at the rate of one reading every two seconds. This reporting rate is 60 times slower than the reporting rate in Example 2.21. The voltage measurements at the unknown phase is plotted in Figures 2.32(a), (b), and (c) against the voltage measurements at each of the three known phases A, B, and C, respectively, for a duration of 15 minutes of measurements. The correlation coefficients are obtained as

$$\begin{aligned} \text{Corr}\,(V_1, V_A) &= 0.9289, \\ \text{Corr}\,(V_1, V_B) &= 0.9286, \\ \text{Corr}\,(V_1, V_C) &= 0.9751. \end{aligned} \tag{2.35}$$

Therefore, we can conclude that the single-phase load is connected to Phase C. This result is consistent with the outcome of the analysis in Example 2.21.

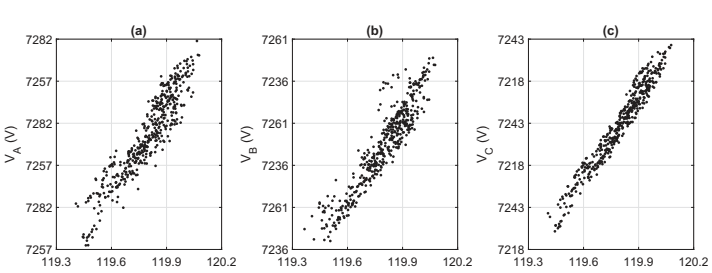

Figure 2.32 Voltage measurements with an unknown phase plotted against the voltage measurements with known phases in Example 2.22: (a) Phase A; (b) Phase B; (c) Phase C.

There are several other ways of solving the phase identification problem depending on the type of smart grid sensor technologies that are available. We will discuss phase identification further in Section 3.6.4 in Chapter 3, Section 5.9.2 in Chapter 5, and Sections 6.2 and 6.7 in Chapter 6.

2.9 Measuring Frequency

Another fundamental characteristic of AC voltage and current signals is frequency. The instrument to measure frequency is the *frequency meter*. Common frequency metering technologies include resonance-type devices, which often have low resolution in the order of 0.25 Hz, as well as time-measurement-based devices, which measure the time interval between two consecutive zero crossings of the voltage waveform. More recently, synchronized phasor measurements are also used to measure power system frequency; see Section 3.3 in Chapter 3. A frequency measurement is more accurate if the signal is sinusoidal with no or little distortion. Therefore, frequency is often measured based on voltage signals, as opposed to current signals that are prone to distortion due to nonlinear loads; see Chapter 4.

An example for frequency measurements during normal grid operating conditions is shown in Figure 2.33. The measurements in this figure are averaged in each second. In North America, frequency is typically maintained at 60 ± 0.036 Hz [132]. The frequency measurements in Figure 2.33 are within this range.

2.9.1 Generation-Load Imbalance

Managing the operation of the electric grid includes a constant effort to *balance* electric power generation with electric power consumption. The impact of unbalance between electric power generation and electric power consumption can be explained based on the *electromechanical* operation of turbine generators.

If electric power consumption exceeds electric power generation, then the turbine generators *slow down* slightly, converting some of their mechanical kinetic energy (*inertia*) into extra electric power to help meet the increased load. Since the frequency of the generated power is proportional to the turbine's *rotor speed*, increasing electric

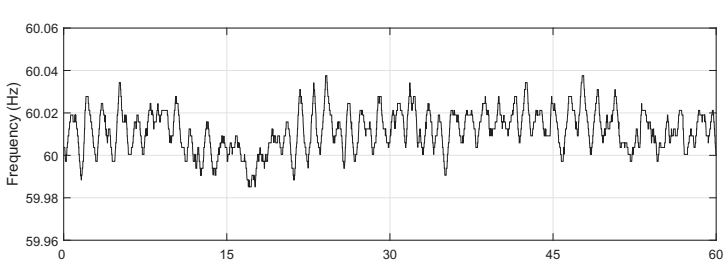

Figure 2.33 Frequency measurements during normal operating conditions.

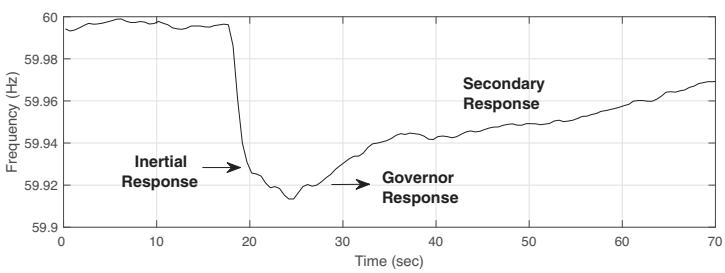

Figure 2.34 Frequency measurements during a major generator loss event.

power consumption results in a drop in the system frequency [3]. It takes a few seconds for a turbine generator to increase its mechanical torque to bring its rotor speed and therefore the system frequency back to normal.

Conversely, if electric power consumption falls below electric power generation, then the turbine generators *speed up* slightly, thus increasing the frequency, before their rotor speed and the system frequency are brought back to normal.

A considerable momentary *under-frequency* operation indicates a considerable momentary generation *deficit*. In contrast, a considerable momentary *over-frequency* operation indicates a considerable momentary generation *surplus*.

Example 2.23 A generator trip can cause a sudden imbalance between generation and load. This can create a sudden drop in frequency, as shown in Figure 2.34, based on a scenario in [133]. Here, a generator trips, and the frequency drops to 59.91 Hz. The rate of frequency drop decays within three to four seconds because of the *inertial response* of the system. For example, when frequency drops, motor loads slow down, which results in less generation-load mismatch. Next, the governor control of generators starts to arrest and then halt the frequency decline within 8–10 seconds. This procedure is known as *primary frequency response*. Finally, the secondary frequency response kicks in by Automatic Generation Control (AGC), which deploys regulating reserves, i.e., the fast-responding generators, to bring the frequency back to the scheduled level.

The exact change in frequency from a lost generator may vary based on the time of day and the season. Nevertheless, one can estimate the amount of frequency decline from a lost generator in a power grid interconnection using the frequency response, also known as the *frequency response characteristic* (FRC), corresponding to that interconnection. FRC indicates the change in frequency as a result of a change in load-generation imbalance. It is calculated using historical frequency measurements during generation and load loss events over several years. The current estimates of FRC for all three North American interconnections are [134]:

- Eastern Interconnection: −2760 MW / 0.1 Hz
- Western Interconnection: −1482 MW / 0.1 Hz
- Texas Interconnection: −650 MW / 0.1 Hz

The negative sign means there is an inverse relationship between generation loss and frequency change. For example, on average, a 1000 MW generation loss in the Western Interconnection causes a frequency change in the order of $-1000 \times 0.1/1482 = -0.067$ Hz. As another example, on average, a 1000 MW load loss in the Eastern Interconnection causes a frequency change in the order of $1000 \times 0.1/2760 = 0.036$ Hz. Conversely, FRC can be used to estimate the amount of generator loss from frequency measurements. For example, the size of the lost generator in Example 2.23 is around $-0.085 \times -1482/0.1 = 1260$ MW.

Inertia of Renewable Energy Resources

Frequency measurements can also be used to estimate system inertia [135], examine the impact of renewable generation on frequency response [136], and evaluate the performance of an interconnection to bring frequency back to normal within a five-minute period after a generation loss or a load loss event [133].

2.9.2 Frequency Oscillations

Recall from Section 2.6.1 that wide-area oscillations can affect the magnitude, phase angle, and frequency of voltage. We already saw the impact of wide-area oscillations on voltage magnitude in Example 2.14. Next, we will see the impact of wide-area oscillations on voltage frequency. We will see the impact of wide-area oscillations on voltage phase angle in Section 3.4.3 in Chapter 3.

Example 2.24 Figure 2.35(a) shows a damped oscillation in frequency measurements. The duration of the oscillation is about six seconds. The largest peak-to-peak amplitude during the event is 10 mHz. The frequency of the most dominant oscillation mode is 1.23 Hz. This oscillation event and its frequency could be detected using FFT

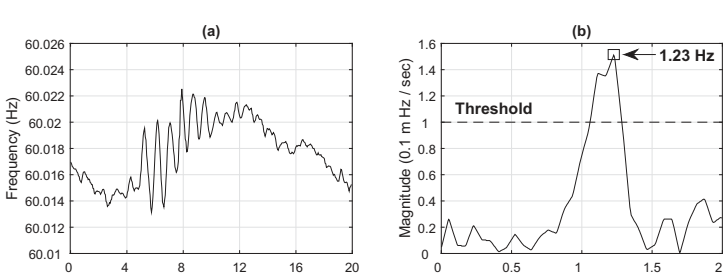

Figure 2.35 Transient oscillations in system frequency: (a) measurements [113]; (b) Fourier analysis. This oscillatory event can be detected by using the FFT method.

analysis, as shown in Figure 2.35(b). The FFT is applied to the differential of the frequency in order to remove its DC offset. Here, the event detection is triggered due to an increase in the FFT magnitude beyond a pre-determined *threshold*. The peak of the FFT magnitude is at 1.23 Hz.

Exercises

2.1 Consider the measurement of RMS current in Example 2.1. Suppose the accuracy of the ammeter that is connected to the secondary side of the CT is $\pm 0.5\%$ `rdg`. What is the possible range of the true current at the primary side of the CT under the following two different scenarios?
(a) The CT is ideal.
(b) The CT is *not* ideal, and its accuracy is $\pm 1\%$.

2.2 The secondary side of a 400:5 CT is connected to an ammeter with burden of 1.47 W and 0.92 VARs, a meter protection relay with a burden of 0.82 W and 0.80 VARs, and a wiring with a burden of 3.60 W and 0.01 VARs. All these elements are connected in series. For all elements, the burden is given at a 5 A–60 Hz secondary current.
(a) How much is the total burden?
(b) Based on Table 2.2, select the burden designation class for this CT.

2.3 The relationship between current I and magnetic field strength B that is measured by a non-contact current sensor in Figure 2.36(a) is expressed as $B = \mu_0 I \cos(\delta)/2\pi r$. Suppose the same sensor is installed on the ground [138], underneath a *balanced* three-phase transmission line in two configurations, as shown in Figures 2.36(b) and (c). Let B_1 and B_2 denote the strength of the magnetic field that is measured by the sensor in each case.
(a) Obtain an expression for B_1 and an expression for B_2.
(b) Express the height of the conductor h as a function of B_1, B_2, and d.

2.4 The working principle of an MOCT is shown in Figure 2.37. The angle of rotation in the polarization is denoted by $\beta = \nu B d$, where ν is a constant and d is the length of the optic tube [79]. If current $i(t)$ in the power cable that creates the magnetic field is a sinusoidal wave, then magnetic field $B(t)$ is also

Table 2.2 IEEE C57.13 Standard burdens for CTs with 5 A secondary winding [137]

Burden Designation	Resistance (Ω)	Inductance (mH)
B-0.1	0.09	0.116
B-0.2	0.18	0.232
B-0.5	0.45	0.580
B-0.9	0.81	1.040
B-1.8	1.62	2.080

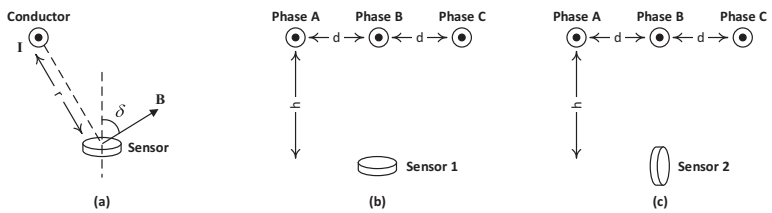

Figure 2.36 Measuring magnetic field strength of conductors in Exercise 2.3.

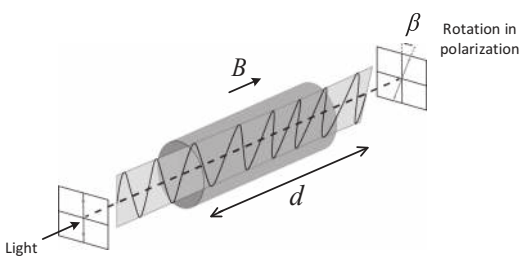

Figure 2.37 The relationship between magnetic field strength B and the amount of rotation in polarization of light that goes through an optic tube; see Exercise 2.4.

a sinusoidal wave; accordingly, $\beta(t)$ is also a sinusoidal wave. Express the RMS value of $\beta(t)$ in terms of the RMS value of $i(t)$.

2.5 The relationship between the magnetic-field-induced voltage $v_s(t)$ in a Rogowski coil in a non-contact current sensor and the current $i(t)$ that flows through the conductor is expressed as follows:

$$v_s(t) = -\frac{AN\mu_0}{l}\frac{di(t)}{dt}, \tag{2.36}$$

where N is the number of turns in the Rogowski coil, A is the area of each turn, l is the length of the winding, and μ_0 is a constant. Suppose $i(t)$ is purely sinusoidal. Express the RMS value of $v_s(t)$ in terms of the RMS value of $i(t)$.

2.6 In Example 2.3, suppose an anti-aliasing filter is designed to filter out any measurement with a frequency above 6 Hz, instead of above 4 Hz.
(a) Is this sufficient to prevent the aliasing scenario in Figure 2.5?
(b) What frequencies may still alias in presence of this anti-aliasing filter?

2.7 From the measurements in Figure 2.6, we have $\Delta V = 285.8 - 285.6 = 0.2$ V and $\Delta I = 145.5 - 136.6 = 8.9$ A. How much is the increase in apparent power load on the one phase that is shown in this figure?

2.8 File `E2-8.csv` contains voltage measurements over a period of 12 hours. The reporting rate of the measurements is *almost* one reading per minute. The first few readings are shown in Figure 2.38. Suppose τ denotes the time difference (in seconds) between any two consecutive readings of voltage.
(a) Calculate τ for all the measurements in the file.
(b) Plot the histogram for τ. Explain your observation.
(c) Is there any *missing* measurement? How many?

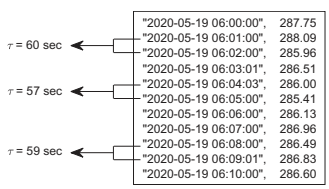

Figure 2.38 Some of the measurements in Exercise 2.8 and examples for calculating τ.

2.9 Suppose there is a momentary voltage spike event, possibly due to a lightning strike, that affects only one cycle. The RMS value of the affected voltage cycle is 145 V. The RMS value of all other cycles is 120 V. Suppose a measurement window of length 4 is used by the voltmeter with *weights* 0.4, 0.3, 0.2, and 0.1, where the highest weight is given to the most recent cycle. The reporting rate of the voltmeter is one RMS value per cycle.

(a) How much is the *peak* of the reported RMS values?

(b) How many of the reported RMS values are affected by the event?

2.10 Two voltage swell events at a distribution feeder are marked with numbers 1 and 2 in Figure 2.39(a). The current on the *same* feeder and the voltage on a *neighboring* feeder are shown in Figures 2.39(b) and (c), respectively. Specify whether each event is a local event or a nonlocal event.

2.11 Consider two neighboring power distribution feeders, and suppose we cross-examine all RMS voltage events above 0.5% rated magnitude. The results based on one month of minute-by-minute RMS voltage measurements are shown in Figure 2.40(a). Each point indicates one event. The location on the x-axis indicates the *change* in voltage on Feeder 1. The location on the y-axis indicates the *change* in voltage on Feeder 2. Suppose we *classify* the event points into eight groups, as shown in Figure 2.40(b). The number of events in each of these eight groups is 107, 102, 67, 0, 106, 104, 65, and 0, respectively.

(a) What percentage of the voltage sag events that are detected on Feeder 1 are caused by the loads and equipment on Feeder 1?

(b) What percentage of the voltage sag events that are detected on Feeder 2 are caused by the loads and equipment on Feeder 2? Compare the results with Part (a).

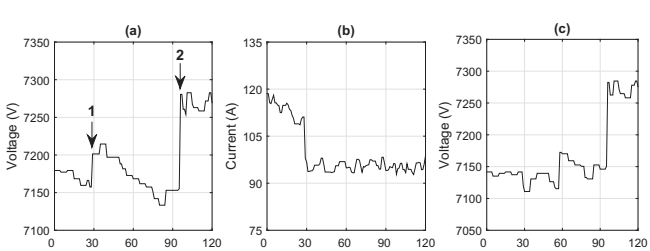

Figure 2.39 Minutely RMS voltage and current measurements in Exercise 2.10.

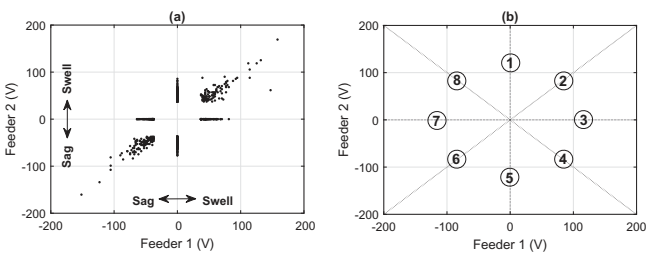

Figure 2.40 Cross-examining voltage events between two feeders in Exercise 2.11 [139].

2.12 File `E2-12.csv` contains the voltage and current measurements, averaged across three phases, at the AC side of a utility-scale PV inverter over a period of one week at one reading per five minutes.
(a) Plot voltage versus current in a scatter plot.
(b) Repeat Part (a) for the measurements between 8 AM and 6 PM. That is, *exclude* the measurements that are obtained *before* 8 AM or *after* 6 PM.

2.13 Consider $n \gg 1$ noise-contaminated samples from signal $x(t)$. Suppose the fixed component of the samples, i.e., their average, is removed. We define:

$$\mathbf{Y} = \begin{bmatrix} x(0) & x(1) & \cdots & x(l) \\ x(1) & x(2) & \cdots & x(l+1) \\ \vdots & \vdots & & \vdots \\ x(n-l-1) & x(n-l) & \cdots & x(n-1) \end{bmatrix}, \tag{2.37}$$

where $l = \lfloor n/2 \rfloor$. The Singular Value Decomposition (SVD) of this matrix is obtained as $\mathbf{Y} = \mathbf{U}\mathbf{\Sigma}\mathbf{V}^T$, where $\mathbf{\Sigma}$ is a diagonal matrix containing the singular values of matrix $\mathbf{Y}$, denoted by $\varsigma_1, \ldots, \varsigma_{l+1}$. The diagonal entries in $\mathbf{\Sigma}$ are sorted in a descending order, i.e., $\varsigma_1 \geq \ldots \geq \varsigma_{l+1}$. A simple noise reduction method works based on setting all singular values that are smaller than ϵ percentage of ς_1 to zero, and then reconstructing samples $x(0), \ldots, x(n)$ from the revised matrix $\mathbf{Y}$. Apply this noise reduction method to the RMS voltage measurements in file `E2-13.csv`. Try $\epsilon = 1\%$ and $\epsilon = 5\%$.

2.14 Consider the *single-mode* oscillation in Figure 2.41. Starting from time $t = 0$, the signal takes the following form: $x(t) = Ae^{\sigma t}\cos(wt + \varphi)$. Obtain the amplitude A, phase angle φ, frequency w, and damping factor σ. You can estimate the frequency by examining the oscillation interval; such as from one positive peak to another positive peak. Other parameters can be estimated similarly by examining various aspects of the signal in the figure.

2.15 In practice, it is common to quantify the damping factor of each oscillatory mode in terms of its *damping ratio*, in percentage, which is obtained as

$$\zeta_i = \frac{-\sigma_i}{\sqrt{\sigma_i^2 + w_i^2}} \times 100\%. \tag{2.38}$$

Obtain the damping ratio for all the oscillatory modes in Table 2.1.

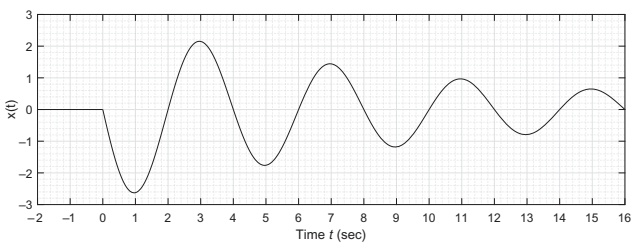

Figure 2.41 Single-mode oscillation in Exercise 2.14. Oscillation starts at time $t = 0$.

2.16 File `E2-16.csv` contains the voltage measurements for the transient oscillations in Figure 2.18. We want to go through the steps to obtain the modes that are shown in Table 2.1. Recall that in Example 2.16 we have $m = 101$.
(a) Obtain vector $\mathbf{\Psi}$ and matrix $\mathbf{X}$.
(b) Solve the LS problem in (2.12) to obtain $a_1, \ldots, a_m$.
(c) Solve the characteristics polynomial in (2.15) to obtain $z_1, \ldots, z_m$.
(d) Use (2.17) to obtain $w_1, \ldots, w_m$ and $\sigma_1, \ldots, \sigma_m$.
(e) Obtain vector $\mathbf{\Phi}$ and matrix $\mathbf{Z}$.
(f) Use (2.19) to obtain $R_1, \ldots, R_m$.
(g) Use (2.20) to obtain $A_1, \ldots, A_m$ and $\varphi_1, \ldots, \varphi_m$.

2.17 Repeat Exercise 2.16, but this time set $m = 201$. Present the oscillation modes in a table similar to Table 2.1.

2.18 The accuracy of the Prony method for any given number of modes m can be evaluated by calculating the *root mean square error* (RMSE) between the original measurements and the Prony estimation of the measurements:

$$\text{RMSE} = \sqrt{\frac{1}{n}\sum_{\tau=1}^{n}\left(x(\tau) - \sum_{i=1}^{m} A_i e^{\sigma_i \tau}\cos(w_i \tau + \varphi_i)\right)^2}. \tag{2.39}$$

(a) Obtain the RMSE for the results in Exercise 2.16.
(b) Obtain the RMSE for the results in Exercise 2.17.

2.19 File `E2-19.csv` contains a voltage profile at a 120 V single-phase load. We want to identify the events in this voltage profile by using the Min-Max method, with a threshold of 2 V. The detection window size is 10.
(a) Use non-overlapping detection windows. List the events that you detect.
(b) Use detection windows with 50% overlap. List the events that you detect.

2.20 Repeat Exercise 2.19, but use the MAD method with $\gamma = 1.4826$ and $\zeta = 3$.

2.21 File `E2-21.csv` contains the minute-by-minute measurements for phase voltages V_A and V_B and line-to-line voltage V_{AB} for a duration of one hour. Plot θ, i.e., the angle between the voltage phasors at Phase A and Phase B, while it changes during the hour; see Eq. (2.27).

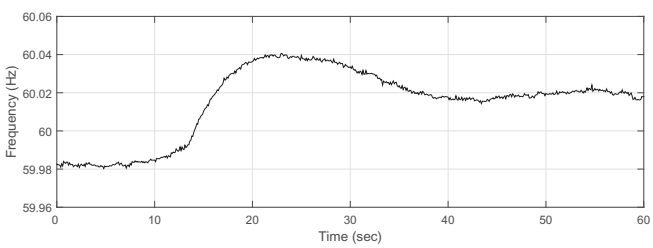

Figure 2.42 Measurements during a system-wide frequency event in Exercise 2.26 [133].

2.22 File `E2-22.csv` contains two sets of second-by-second three-phase voltage measurements that are taken at two close-by locations on the same circuit. The phases for the first set of measurements are labeled as A, B, and C. The phases for the second set of measurements are labeled as a, b, and c.

(a) Obtain the correlation coefficients across all phases, i.e., between Phase A and Phase a, between Phase A and Phase b, between Phase A and Phase c, etc. A total of *nine* correlation coefficients should be calculated.

(b) Solve the phase identification problem. That is, take phases A, B, and C as reference and identify the phase connectivity for Phases a, b, and c.

2.23 File `E2-23.csv` contains minute-by-minute three-phase voltage measurements at a load location over a period of one week.

(a) Plot the histogram of the PU during this week.

(b) Does PU exceed 1% at any time?

2.24 File `E2-24.csv` contains the frequency measurements for duration of one day at one reading per second. Nominal frequency is 60 Hz.

(a) Plot the histogram for these measurements at 0.01 Hz resolution.

(b) What percentage of the measurements are outside the 60 ± 0.036 range?

(c) Plot the frequency during the event in which it drops below 59.95 Hz. How long does the frequency stay below $60 - 0.036$ Hz during this event?

2.25 Based on their FRC values, the system frequency in which North American interconnection is likely to be *least* affected by losing a 500 MW generator?

2.26 Consider the frequency measurements in Figure 2.42.

(a) Suppose the measurements are done in California. Explain the reason for the surge in frequency during the 10th and the 20th seconds. In particular, estimate the amount of change (in MW) of generation or consumption.

(b) Suppose the measurements are done in Texas. Repeat Part (a).

2.27 Consider an energy storage unit with 1.5 MWh energy rating and 250 kW power rating. Suppose this storage unit is used to regulate frequency. The storage unit is discharged whenever the frequency drops below $60 - 0.036 = 59.964$ Hz; see Figure 2.43(a). The storage unit is charged whenever the frequency exceeds above $60 + 0.036 = 60.036$ Hz; see Figure 2.43(b). Suppose the storage

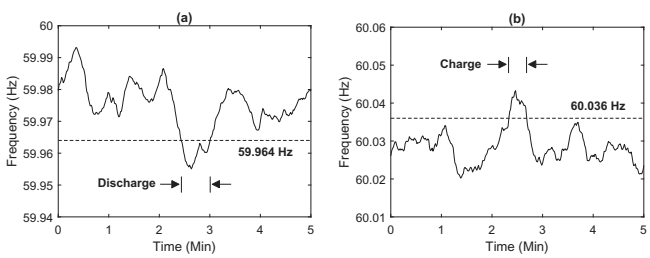

Figure 2.43 Operation of the energy storage unit in response to changes in frequency in Exercise 2.27: (a) charge the storage unit when the frequency drops below a threshold; (b) discharge the storage unit when the frequency exceeds above a threshold.

unit responds to the second-by-second frequency measurements in file `E2-27.csv`. The initial state of charge (SoC) is 50%.

(a) Identify all the charge intervals and all the discharge intervals.

(b) Suppose the storage unit is ideal. Plot the SoC curve versus time.